Investigation of the homogeneity of energy conversion processes at dipolarization fronts from MMS measurements

S. W. Alqeeq, O. Le Contel, Patrick Canu, Alessandro Retinò, Thomas Chust,
Laurent Mirioni, L. Richard, Y. Aït-Si-Ahmed, A. Alexandrova, A. Chuvatin,
et al.

AUTHOR QUERY FORM

AIP Publishing	**Journal: Phys. Plasmas** **Article Number: POP21-AR-MMS2021-01348**	**Please provide your responses and any corrections by annotating this PDF and uploading it to AIP's eProof website as detailed in the Welcome email.**

Dear Author,

Below are the queries associated with your article; please answer all of these queries before sending the proof back to AIP.

Article checklist: In order to ensure greater accuracy, please check the following and make all necessary corrections before returning your proof.

1. Is the title of your article accurate and spelled correctly?

2. Please check affiliations including spelling, completeness, and correct linking to authors.

3. Did you remember to include acknowledgment of funding, if required, and is it accurate?

Location in article	Query / Remark: click on the Q link to navigate to the appropriate spot in the proof. There, insert your comments as a PDF annotation.
AQ1	Please check that the author names are in the proper order and spelled correctly. Also, please ensure that each author's given and surnames have been correctly identified (given names are highlighted in red and surnames appear in blue).
AQ2	Please define LHDI at first occurrence.
AQ3	Please specify which sections "in the next sections" refer to in the sentence beginning "They are mentioned as they …."
AQ4	In sentence beginning "One can see that electrons …," please confirm that "the next section" refers to Sec. VI.
AQ5	In sentence beginning "Conversely, the current density remains…," please confirm that "next section" refers to Sec. VII.
AQ6	Refs. 58 and 59 were not cited in your original manuscript. We have inserted a citation for them in the sentence beginning "This latter contribution can be…." Please carefully review our placement of the citation and confirm that it is correct. If it is not correct, mark the citation for deletion and specify where the citation for Refs. 58 and 59 should be inserted.
AQ7	Please provide publisher name for Ref. 44.
AQ8	We were unable to locate a digital object identifier (doi) for Ref(s). 5, 8, 10, 18, 29, 45, and 48. Please verify and correct author names and journal details (journal title, volume number, page number, and year) as needed and provide the doi. If a doi is not available, no other information is needed from you. For additional information on doi's, please select this link: http://www.doi.org/.
AQ9	Please provide journal title for Ref. 55.
	Please confirm ORCIDs are accurate. If you wish to add an ORCID for any author that does not have one, you may do so now. For more information on ORCID, see https://orcid.org/. S. W. Alqeeq - 0000-0002-5401-6644 O. Le Contel - 0000-0003-2713-7966

P. Canu-

A. Retinò-

T. Chust-

L. Mirioni-

L. Richard-

Y. Aït-Si-Ahmed-

A. Alexandrova-

A. Chuvatin-

N. Ahmadi - 0000-0001-5267-0485

S. M. Baraka - 0000-0001-6748-6795

R. Nakamura - 0000-0002-2620-9211

F. D. Wilder-

D. J. Gershman - 0000-0003-1304-4769

P. A. Lindqvist - 0000-0001-5617-9765

Yu. V. Khotyaintsev - 0000-0001-5550-3113

R. E. Ergun-

J. L. Burch - 0000-0003-0452-8403

R. B. Torbert-

C. T. Russell-

W. Magnes-

R. J. Strangeway-

K. R. Bromund-

Hanying Wei-

F. Plaschke-

B. J. Anderson-

B. L. Giles-

S. A. Fuselier-

Y. Saito-

B. Lavraud-

Thank you for your assistance.

Investigation of the homogeneity of energy conversion processes at dipolarization fronts from MMS measurements

AQ1

S. W. Alqeeq,[1,a] O. Le Contel,[1] P. Canu,[1] A. Retinò,[1] T. Chust,[1] L. Mirioni,[1] L. Richard,[2,3] Y. Aït-Si-Ahmed,[1] A. Alexandrova,[1] A. Chuvatin,[1] N. Ahmadi,[4] S. M. Baraka,[5] R. Nakamura,[6] F. D. Wilder,[7] D. J. Gershman,[8] P. A. Lindqvist,[9] Yu. V. Khotyaintsev,[2] R. E. Ergun,[4] J. L. Burch,[10] R. B. Torbert,[11] C. T. Russell,[12] W. Magnes,[6] R. J. Strangeway,[12] K. R. Bromund,[8] Hanying Wei,[12] F. Plaschke,[6] B. J. Anderson,[13] B. L. Giles,[8] S. A. Fuselier,[10] Y. Saito,[14] and B. Lavraud[15]

AFFILIATIONS

[1]Laboratoire de Physique des Plasmas (LPP), UMR7648, CNRS, Sorbonne Université, Université Paris-Saclay, Observatoire de Paris, Ecole Polytechnique Institut Polytechnique de Paris, Paris 75005, France.
[2]Swedish Institute of Space Physics, Uppsala 75236, Sweden
[3]Department of Physics and Astronomy, Uppsala University, Uppsala 75236, Sweden
[4]Laboratory for Atmospheric and Space Physics, University of Colorado, Boulder, Colorado 80303, USA
[5]National Institute of Aerospace, Hampton University, Hampton, Virginia 23666, USA
[6]Space Research Institute, Austrian Academy of Sciences, Graz 8042, Austria
[7]Physics Faculty, University of Texas, Arlington, Texas 76019, USA
[8]NASA Goddard Space Flight Center, Greenbelt, Maryland 20771, USA
[9]Royal Institute of Technology, Stockholm 11428, Sweden
[10]Southwest Research Institute, San Antonio, Texas 78238, USA
[11]Space Science Center and Department of Physics, University of New Hampshire, Durham, New Hampshire 03824, USA
[12]Department of Earth, Planetary and Space Sciences, University of California, Los Angeles, California 90095, USA
[13]Applied Physics Laboratory, The Johns Hopkins University, Laurel, Maryland 20723, USA
[14]Institute for Space and Astronautical Science, Sagamihara, Kanagawa 252-5210, Japan
[15]Institut de Recherche en Astrophysique et Planétologie (IRAP), CNRS UMR5277/Université Paul Sabatier, Toulouse 31400, France

Note: This paper is a part of the Special Collection: Plasma Physics from the Magnetospheric Multiscale Mission.
[a]**Author to whom correspondence should be addressed:** alqeeq@lpp.polytechnique.fr

ABSTRACT

We report on six dipolarization fronts (DFs) embedded in fast earthward flows detected by the Magnetospheric Multiscale mission during a substorm event on 23 July 2017. We analyzed the Ohm's law for each event and found that ions are mostly decoupled from the magnetic field by the Hall fields. However, the electron pressure gradient term is also contributing to the ion decoupling and likely responsible for an electron decoupling at DF. We also analyzed the energy conversion process and found that the energy in the spacecraft frame is transferred from the electromagnetic field to the plasma ($\mathbf{J} \cdot \mathbf{E} > 0$) ahead or at the DF, whereas it is the opposite ($\mathbf{J} \cdot \mathbf{E} < 0$) behind the front. This reversal is mainly due to a local reversal of the cross-tail current indicating a substructure of the DF. In the fluid frame, we found that the energy is mostly transferred from the plasma to the electromagnetic field ($\mathbf{J} \cdot \mathbf{E}' < 0$) and should contribute to the deceleration of the fast flow. However, we show that the energy conversion process is not homogeneous at the electron scales due to electric field fluctuations likely related to lower-hybrid drift waves. Our results suggest that the role of DF in the global energy cycle of the magnetosphere still deserves more investigation. In particular, statistical studies on DF require to be carried out with caution due to these electron scale substructures.

Published under an exclusive license by AIP Publishing. https://doi.org/10.1063/5.0069432

I. INTRODUCTION

Fast plasma flows in the magnetotail have been investigated for a long time thanks to *in situ* space measurements. They contribute significantly to the energy, plasma, and magnetic flux transports in the Earth's magnetosphere.[1–4] They are thought to be generated by magnetic reconnection,[5–7] kinetic ballooning interchange instability,[8] or low entropy magnetic flux tubes;[9] they can be related to a global scale substorm activity or appear as isolated structures. Dipolarization fronts (DFs), which are mostly characterized by a sharp and transient increase in the normal component (northward) of the magnetic field in the magnetotail, are formed by the plasma flow propagation or can be also embedded in the flow. The sharp increase in the magnetic field is often interpreted as the magnetic field pile up behind the front. These fronts can be also preceded by a decrease in the normal component.[10–12] The whole spatial scale of DF is about few ion inertial lengths (c/ω_{pi}, where ω_{pi} is the ion plasma frequency).[13–15] A recent review by Fu *et al.* has focused on their important role in particle acceleration mechanisms.[16]

Angelopoulos *et al.* suggested that the DF could play an important role in the energy conversion process due to their large scale propagation through the Earth's magnetosphere.[17] Based on data from the THEMIS mission, they showed that energy conversion occurs within an electron scale current sheet (1–10 electron inertial lengths) generated by DF propagation. Integrated all along the propagation mostly along the X geocentric solar magnetospheric (GSM) direction and assuming a transverse Y–Z section of about 10 R_E^2, the authors suggested that DFs are able to provide a macroscopic energy conversion. Therefore, the estimate of the energy conversion at DFs seems to be crucial to understand the global energy cycle in the Earth's magnetosphere.

This question is also fundamental for the fast flow propagation itself. Indeed, as the fast flow propagates, the fraction of energy that it can lose due to various energy conversion processes contributes to its braking. Using THEMIS data, Chaston *et al.*[18] suggested that kinetic Alfvén waves continually radiated toward the auroral region by fast flows during their earthward propagation can extract the total kinetic energy from the flows. Later Hamrin *et al.*[19] found indications of fast flow decelerations in the range $-25 < X < -15$ R_E and investigated the related energy conversion processes by computing the $\mathbf{J} \cdot \mathbf{E}$ term where ($\mathbf{J}$ is the current density and $\mathbf{E}$ the electric field in the spacecraft frame). Thanks to a superposed epoch analysis applied on Cluster data, they found that fast flows with a velocity peak behind the front are decelerated and that energy is radiated, i.e., converted from particles to fields, whereas, when the velocity peak is detected ahead or at DF, no braking signature is detected and energy is transferred from fields to particles (dissipation). Still from statistical analysis of 2003 Cluster data corresponding to an average subproton scale spacecraft separation of 200 km, Huang *et al.*[20] found that the energy was significantly transferred from the fields to the plasma at DFs. More recently, using data gathered during the Magnetospheric Multiscale (MMS) commissioning phase and with a better time resolution for particle measurements (150 ms for ions, 30 ms for electrons), Yao *et al.*[21] showed that electron contribution to the DF current density is significant (60% of ions) and produced by the diamagnetic effect. With regard to the energy conversion, they found that the field energy is transferred to the plasma in the spacecraft frame though the velocity peak is detected behind the DF. In the fluid frame (ion or electron),

they pointed out that the energy transfer is from particles to fields. Later Liu *et al.*[22] showed that ion scale DFs can be also associated with electron scale current sheets. They specify that although their DF event corresponded primarily to an energy transfer from fields to particles, the electron scale currents could also lead to radiating the plasma energy. Such electron scale DF substructures were also reported in previous studies and attributed to the lower-hybrid drift instability growing in the density gradient region[23–26] leading to ripples on the DF.[27] Later, these results were confirmed by a statistical study carried out by Zhong *et al.*[28] based on 122 DF events detected by MMS in the magnetotail. The contribution of broad band high-frequency waves (with frequencies between the electron gyrofrequency and the plasma frequency) was also investigated and shown to be up to 10% of the total energy conversion at DF.[26] Finally, Zhang *et al.*[29] suggested that both Joule dissipation via parallel and perpendicular currents and radiated energy by kinetic Alfvén waves contribute to the fast flow slowdown.

Energy conversion processes have also been investigated recently by 3D kinetic particle-in-cell (PIC) simulations. The role of the lower-hybrid drift instability rising at DFs was also investigated and pointed out as a significant element of the DF dynamics.[30] Later, comparing 3D PIC simulation results and Cluster observations Khotyaintsev *et al.* concluded that the energy dissipation in the satellite (Earth) frame was mainly due to the motional electric field and the ion contribution to the current, suggesting that LHDI was not contributing to the energy conversion process. They found almost no energy conversion in the DF frame (defined by using the ion velocity at the DF).[31] Using recent theoretical developments in turbulence studies by Yang *et al.*,[32] which allow to disentangle ion and electron contributions, Sitnov *et al.*[33] showed that ions are heated at and ahead of DFs, whereas electrons are heated at and behind due to the long-wavelength lower-hybrid drift instability; therefore, both contributions lead to an important energy dissipation. Finally, Nakamura *et al.*[34] also carried out 3D PIC simulations and reported that energy is dissipated in the electron frame at DFs within the density gradient layer due to the lower-hybrid instability. Their numerical results were shown to be in good agreement with the recent MMS observations described by Liu *et al.* although the energy conversion term was estimated in the electron frame for the simulations and in the satellite frame for the observations.[22]

In the present study, we investigate the energy conversion processes for six DFs embedded in fast earthward flows detected by MMS on 23 July 2017. Data and methods are described in Sec. II. An overview of basic DF properties is presented in Sec. III. In Sec. IV, we present a cross-validation of current density calculations and of Hall electric fields. Ion and electron dynamics are investigated thanks to the Ohm's law in Sec. V; then, the energy conversion processes at the vicinity of these six DFs are scrutinized in Sec. VI. Finally, we summarize and discuss the global results of this study in Sec. VII.

II. DATA AND METHODS
A. Data

In the present study, we analyze the various physical quantities measured by the MMS instrument suite.[35,36] DF properties are characterized thanks to the magnetic field measurements provided by the fluxgate magnetometer (FGM) with a sampling frequency of 128 Hz in burst mode,[37] the electric field measurements (EDP) sampled at 32 Hz in fast survey mode,[38,39] the ion and electron moment

AQ2

Physics of Plasmas　　　　　　　　　ARTICLE　　　scitation.org/journal/php

measurements provided by the fast plasma investigation suite (FPI) sampled at 150 and 30 ms, respectively.[40] However, due to the very low density in the magnetotail (<0.05 part·cm^{-3}), we have used the electron partial moments provided by the FPI team for which the integration of the distribution function starts at the minimum energy of 100 eV. Furthermore, in order to reduce even more the noise on electron moments, we have time averaged the electron data at 0.3 s. Hence, all results shown in this study are based on data with a 0.3 s time resolution. Background noise produced by energetic electrons penetrating the ion detectors has been subtracted from ion FPI measurements as recommended by the FPI team.[41] The upper energy limit of FPI is 30 keV; therefore, ion moment calculations can be still inaccurate in the magnetotail where ions can be more energetic, as we will see by comparing them with the particle measurements from the hot plasma composition analyzer (HPCA), which has a higher energy cut-off and a time resolution of 10 s.[42]

Throughout the paper, current densities from FPI measurements ($\mathbf{J}_{part} = en_e(\mathbf{v}_i - \mathbf{v}_e)$) are computed using single spacecraft data, which have been time averaged at 0.3 s. Also, we compute a four-spacecraft average of these single satellite current densities in order to compare with the current estimated from the curlometer technique[43] given by $\mathbf{J}_{curl} = (\nabla \times \mathbf{B})/\mu_0$. This comparison allows us to verify the reliability of the particle moments despite the instrumental issues mentioned above. The use of HPCA proton moments in the current density calculations does not modify the results as the current is most of the time dominated by the electron motion.

Finally, data used in the present study were gathered by MMS on the 23 July 2017 when the constellation was located on the dusk side of the magnetotail [X $= -23.9$, Y $= 5.8$, Z $= 5.4$] Earth radii (R$_E$) in the geocentric solar ecliptic coordinate system (GSE). The average spacecraft separation was about 15 km, i.e., close to the scale of the average electron Larmor radius during this period (in average between 40 and 60 km).

Between 16:45 and 17:15 UT, MMS detected successive fast earthward flows, which occurred during a substorm period as indicated by the auroral electrojet—AE index ~400 nT (courtesy of Kyoto World data Center for Geomagnetism: http://wdc.kugi.kyoto-u.ac.jp/ae_provisional/201707/index_20170723.html).

In Sec. III, six DF signatures embedded in these fast flows are described.

B. Methods

DFs can be described locally (at the scale of a single satellite) as 1D tangential discontinuities.[11,23] Therefore, DF signatures are usually displayed in a local coordinate system obtained from a minimum variance analysis[44] applied on magnetic fields data (MVAB) of a single spacecraft[20,22] and/or from a timing analysis in case of a multi-spacecraft missions.[45] MVAB is applied over the time period corresponding to the sharp increase of northward component (B_z) of the four spacecraft average of the magnetic field measurement. MVAB applied on single spacecraft magnetic field data gives similar LMN frames. Note that when additional structures ahead or behind the DF are identified, they are excluded to the time period used for MVAB.

III. OVERVIEW OF CLASSICAL DF PROPERTIES

In this section, we describe the global properties of six DF events, each one embedded in a fast earthward flow detected by MMS between 16:45 and 17:15 UT.

Figure 1 shows these six DF events denoted DF1, DF2a,b, DF3a,b, and DF4 in their respective LMN frame obtained from the MVAB. For each event, the MVAB results are summarized in Table I, and the time period used is indicated. From these MVAB results, we define L, M, and N vectors as maximum, intermediate, and minimum variance directions, respectively. We have verified that the ratio between the three corresponding eigenvalues, $\lambda_1, \lambda_2, \lambda_3$, is sufficiently large (>10 in average though three ratios are between 2 and 10) to indicate that the three directions are well separated (see Table I). Table II shows the components of the normal estimated by a timing analysis as well as the velocity along the normal in GSE. The estimated thickness δ of each DF event is also given (in km and in d$_i$, the ion inertial length estimated based on the plasma sheet density prior to respective DF arrival) by multiplying the normal DF velocity by the time interval between the minimum and maximum of B_L.[31] Note that in accordance with the propagation direction given by timing analysis, the orientation of the N vector of the MVAB was set to be positive (earthward) and L always oriented northward leading to M directed dawnward. Normal directions obtained from the two methods are qualitatively consistent and indicate that DFs are mainly oriented earthward (along X GSE), some DFs having a significant duskward component (along Y GSE) and southward component (along $-Z$ GSE). DF normal velocities range from 135 to 481 km/s. As the angle between the DF2a and DF2b normals (respectively, DF3a and DF3b) is ~12.7° (respectively, ~22.2°), and for the sake of simplicity, only DF2a and DF3a LMN frames are used for plotting DF2 and DF3 periods. We checked that similar results are obtained when individual LMN frames are used. The estimated thickness of the DFs ranges from 0.98 to 3.78 d$_i$ as found in previous THEMIS,[11] Cluster,[14,46] and MMS[15,21,22,31] studies.

Figure 1 displays ion scale properties of these six DFs. Magnetic field components and magnitude are plotted in Fig. 1(a), FPI ion velocity components and the N component of the HPCA velocity (V_{H+}) are shown in Fig. 1(b), ion and electron temperatures are shown in Fig. 1(c), electron density us shown in Fig. 1(d), and finally ion and electron pressure variations are shown in Fig. 1(e). These six DF events are identified by a vertical red dashed line (maximum of the B_L component). Vertical black dashed lines indicate possible signatures of flux ropes (large increase in the total magnetic field due to an increase in the cross-tail M component, associated with a bipolar signature of another component) ahead of these DF signatures. The detailed description of these flux ropes is beyond the scope of this study. They are mentioned as they can drive their own energy conversion processes as we will see in the next sections.

AQ3

The six DF signatures can be considered to belong to category A, the most common category, of the DF classification established from a statistical study based on 303 events detected by the Cluster mission.[12] Indeed, the latter study created four large categories to which DF is linked according to their magnetic field, ion density, velocity, temperature, and pressure variations during the DF crossing. Category A, the most common, corresponds to DFs with a density decrease [see Fig. 1(d)] and a temperature increase [see Fig. 1(c)] consistent with the transition between a relatively cold dense plasma at rest with respect to a hot tenuous fast moving plasma. Note that the HPCA V_N velocity is always much larger than FPI V_N [see Fig. 1(b)], confirming that FPI instrument underestimates the velocity of the earthward flow due to

Physics of Plasmas   ARTICLE   scitation.org/journal/php
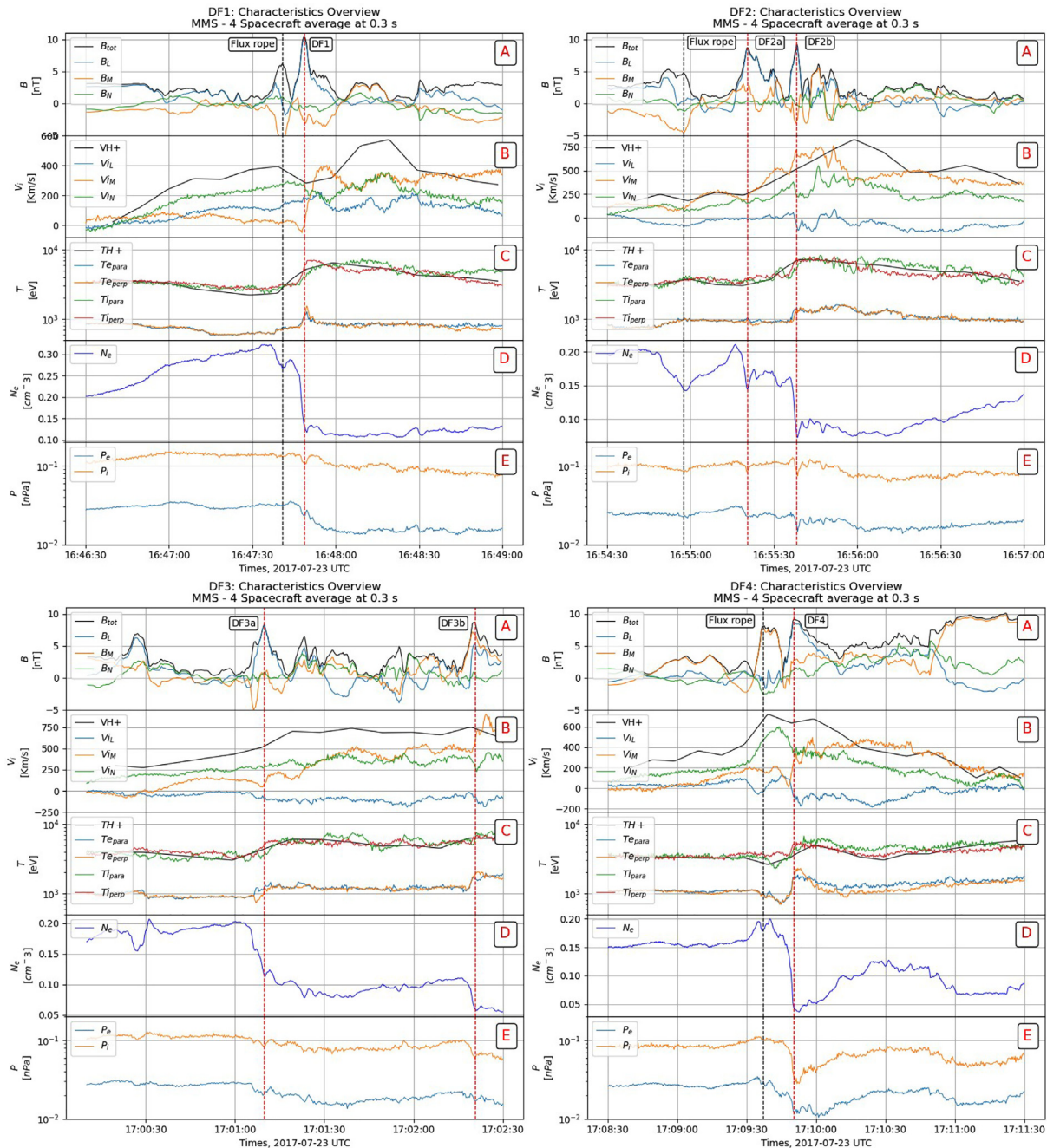

FIG. 1. Six DF signatures (vertical red dashed line) denoted DF1, DF2a,b, DF3a,b, DF4 in their respective LMN frame, all data are averaged over the four satellites then time averaged at 0.3 s. For each event, panel (a) shows the magnetic field components and its magnitude, (b) the components of ion velocity from FPI and the N component of the V_{H+} HPCA velocity, (c) the electron and ion temperatures from FPI with the isotropic proton temperature from HPCA, (d) the electron density, (e) the ion and electron pressures from FPI. Vertical black dashed lines indicate possible flux rope signatures (see text).

its limited upper energy. Moreover, the maximum of the V_N component of the ion velocity is always located behind the DF associated with the maximum of B_L, which according to Hamrin et al.[19] results should, therefore, correspond to decelerated DFs with a significant part of the energy being radiated. Furthermore, in such conditions, Fu et al. showed that these DFs correspond to growing magnetic flux pile-up region (innermost flux tubes being pushed by faster outermost flux tubes leading to the compression of the magnetic field) causing the

Physics of Plasmas   ARTICLE   scitation.org/journal/php

TABLE I. Minimum variance analysis (MVAB) results: Eigen value ratios and vectors (in GSE).

DF	UT	$\frac{\lambda_M}{\lambda_N}$	$\frac{\lambda_L}{\lambda_N}$	L	M	N
DF1	16:47:45/16:47:50	5.69	450.62	0.14, 0.63, 0.76	0.13, −0.78, 0.62	0.98, 0.01, −0.19
DF2a	16:55:10/16:55:25	75.67	813.54	0.06, 0.47, 0.88	0.64, −0.70, 0.33	0.77, 0.54, −0.34
DF2b	16:55:35/16:55:36	19.6	14218.5	0.08, 0.72, 0.69	0.60, −0.59, 0.54	0.8, 0.37, −0.48
DF3a	17:01:03/17:01:09	42.25	103.88	0.01, 0.59, 0.81	0.61, −0.64, 0.47	0.79, 0.49, −0.36
DF3b	17:02:18/17:02:19	29.62	186.86	0.6, −0.52, 0.61	−0.20, −0.83, −0.52	0.78, 0.19, −0.60
DF4	17:09:45/17:09:52	58.12	581.82	0.32, 0.06, 0.95	0.77, −0.61, −0.22	0.56, 0.79, −0.24

TABLE II. Timing analysis results: Normal vectors and velocity (in GSE) with estimated DF thickness δ.

DF	UT	(n_x, n_y, n_z)	(Vn_x, Vn_y, Vn_z)	Vn (km/s)	δ (km)	δ (d_i)
DF1	16:47:45/16:47:50	0.95, 0.30, −0.09	186, 59, −18	196	588	1.34
DF2a	16:55:10/16:55:25	0.95, 0.27, −0.13	129, 36, −17	135	811.98	1.63
DF2b	16:55:35/16:55:36	0.86, 0.17, −0.48	241, 49, −135	281	561.42	0.98
DF3a	17:01:03/17:01:09	0.60, 0.72, −0.35	289, 345, −169	481	1924.92	3.78
DF3b	17:02:18/17:02:19	0.34, 0.30, −0.89	124, 111, −327	367	587.536	0.81
DF4	17:09:45/17:09:52	0.54, 0.83, −0.14	251, 390, −63	468	1871.72	3.67

acceleration of electrons by the betatron effect.[47] Finally, from Fig. 1(e), one can see that for electrons, the DF always corresponds to a transition between a high pressure to a low pressure region, whereas for the ions, it mostly corresponds to a transient pressure reduction except for DF4. Therefore, at the DF crossing, the electron pressure gradient can be expected to increase strongly.

IV. CURRENT DENSITY AND HALL ELECTRIC FIELD COMPARISONS

As mentioned in Sec. II, plasma conditions in the magnetotail can make the particle moment measurements difficult. One way to verify the reliability of these measurements is to compare the current densities computed from ion and electron moments averaged over the four individual spacecraft with those estimated independently from the magnetic field data at the same time resolution (0.3 s) using the curlometer technique. Figure 2 shows such comparisons for the current densities ($\mathbf{J}_{part} = en_e(\mathbf{v}_i - \mathbf{v}_e)$ vs $\mathbf{J}_{curl} = (\nabla \times \mathbf{B})/\mu_0$) and the Hall electric fields ($\mathbf{J}_{part} \times \mathbf{B}/(ne)$ vs $\mathbf{J}_{curl} \times \mathbf{B}/(ne)$) estimated for each DF event in their own LMN frame. Figures 2(a)–2(c) for each event demonstrate good agreement between the two current density measurements within an accuracy of about <10 nA/m^2. Indeed, considering an accuracy of 0.1 nT for the magnetic field measurement,[37] the accuracy of the current density measurements from the curlometer with a spacecraft separation of 15 km can be roughly estimated to 5 nA/m^2. The current density accuracy from the particle measurement is estimated to 8 nA/m^2 (see Sec. VI for more details). In similar manner, Figs. 2(d)–2(f) confirm that Hall fields estimated from both currents are in good agreement, within an accuracy of 1 mV/m. However, a large discrepancy between the two Hall field calculations can be found in the low density region and when current densities are smaller than or close to their error bars and oscillate around 0. In such conditions, the error on the current density measurement is amplified by the low density and leads to a large error on the Hall field calculation [e.g., Fig. 2(e), for DF4].

Furthermore, we can identify each DF with their negative peak in J_M (increase in cross-tail duskward current) associated with the bipolar signature of the N component of the Hall electric field. This latter is mostly produced by the reversal of J_M just behind the DF, B_L remaining positive [see Figs. 2(a) and 2(b)]. This Hall field is expected due to the ion inertial scale of the DF, which leads ions to be decoupled from the magnetic field. However, its reversal seems to be related to an electron scale current density shear flow at the DF or to a possible electron vortex signature.

V. ANALYSIS OF OHM'S LAW

The precise analysis of all terms in the generalized Ohm's law, estimated from *in situ* measurements, allows us to identify the regions where the plasma decouples from the magnetic field and kinetic effects become important. It also leads to a better understanding of which term plays the most important role in the energy conversion process. Previous analyses related to fast plasma flows in the magnetotail have been carried out using measurements from the four Cluster satellites (4 s time resolution).[48] The authors suggested that anomalous resistivity term arising from electromagnetic field fluctuations and Hall term played a dominant role in the breakdown of the frozen-in condition. Using both single and multi-satellite methods, it was confirmed that Hall and electron pressure gradient terms contribute to ion decoupling at DF although Hall term was indeed dominant.[14] High time and spatial MMS resolutions allow analysis of Ohm's law at kinetic scales, which are relevant at DF.[21,22] Assuming a possible anomalous resistivity η for collisionless plasmas, the generalized Ohm's law is written as
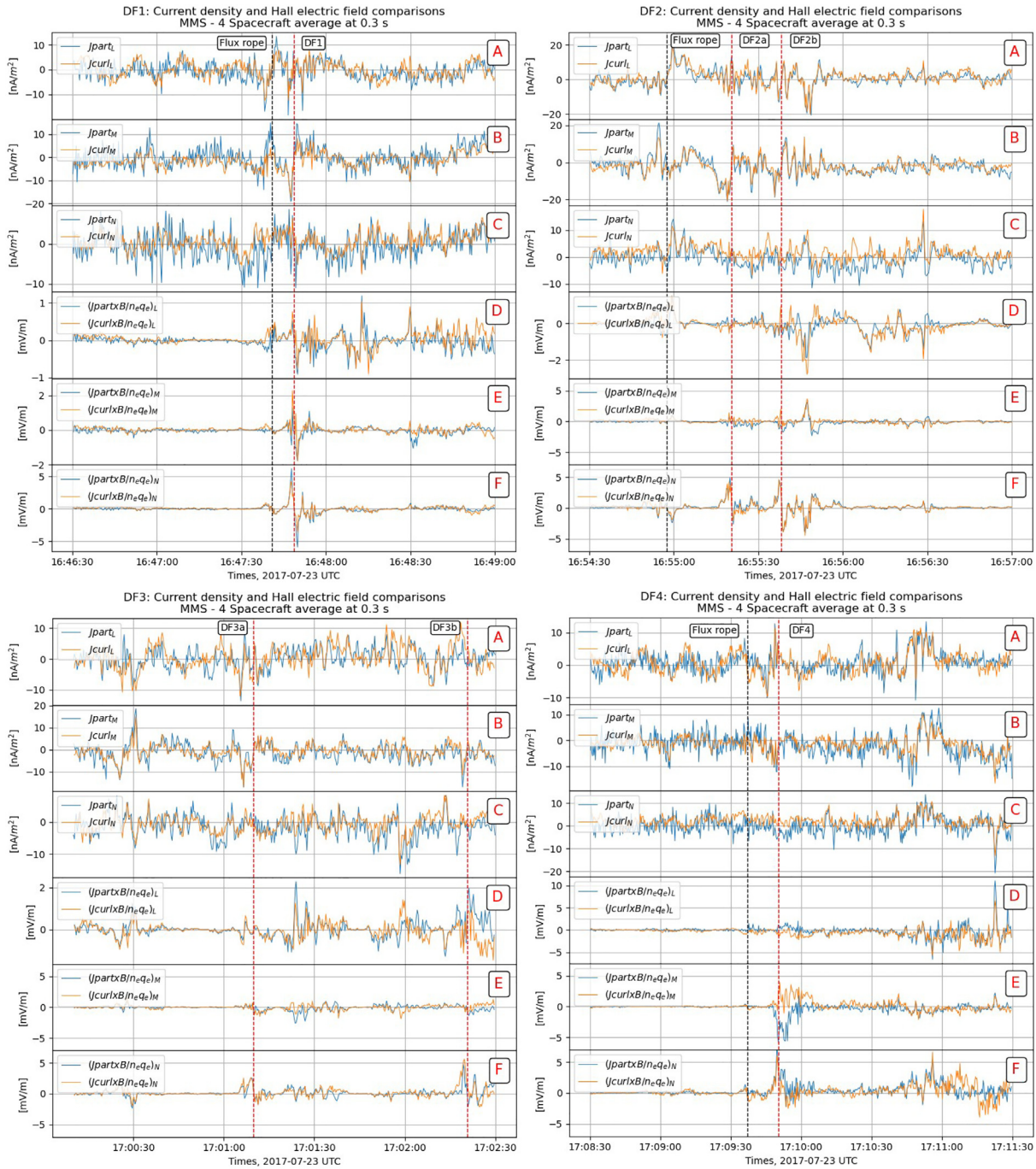
FIG. 2. For each DF event in its respective *LMN* frame, comparison between current densities calculated by using $\mathbf{J}_{part} = en_e(\mathbf{v}_i - \mathbf{v}_e)$ and $\mathbf{J}_{curl} = \nabla \times \mathbf{B}/\mu_0$: (a) along *L*, (b) along *M*, (c) along *N*, and Hall electric field comparison between two computations $\mathbf{J}_{part}/(en_e)$ and $\mathbf{J}_{curl}/(en_e)$: (d) along *L*, (e) along *M*, and (f) along *N*.

$$\mathbf{E} + \mathbf{v_e} \times \mathbf{B} = -\frac{1}{en}\nabla \cdot \mathbf{P_e} - \frac{m_e}{e}\frac{d\mathbf{v_e}}{dt} + \eta\mathbf{J}, \qquad (1)$$

where $\mathbf{v_e}$, $\mathbf{P_e}$ are the electron velocity and pressure tensor, respectively. One writes equivalently

$$\mathbf{E} + \mathbf{v_i} \times \mathbf{B} = \frac{\mathbf{J} \times \mathbf{B}}{en} - \frac{1}{en}\nabla \cdot \mathbf{P_e} - \frac{m_e}{e}\frac{d\mathbf{v_e}}{dt} + \eta\mathbf{J}, \qquad (2)$$

where $\mathbf{v_i}$ is the ion velocity.

In the dayside region, where the plasma density is on average larger than in the magnetotail and at the vicinity of the electron

diffusion region, all terms can be estimated with good accuracy and the validity of the Ohm's law can be tested. Pressure gradient and inertial terms are found to have significant contributions without excluding the existence of an anomalous resistivity term due to high-frequency electric field fluctuations.[49] In the low density magnetotail ($<$1 part·cm^{-3}) and in the vicinity of DFs, electron pressure gradient and inertial terms are difficult to estimate and quite noisy even after time averaging.[22] For each DF event, we have computed both terms. The inertial term is negligible, whereas the divergence of the electron pressure tensor is larger, but still very noisy. Therefore, in the rest of the study, only convective and Hall terms are shown. No anomalous resistivity will be considered, yet the electron pressure gradient term will be estimated by a single satellite method. All data are averaged over the four satellites.

Figure 3 shows the comparison between the ideal ion frozen-in ($\mathbf{E} + \mathbf{v}_i \times \mathbf{B}$) and the Hall electric field ($\mathbf{J}_{part} \times \mathbf{B}/(en)$) terms in LMN coordinates. For all events, ions are decoupled in the vicinity of the DF by the Hall electric field. However, the difference between the two terms can exceed 2 mV/m, which suggests that electron pressure gradient term is not negligible in these regions despite the difficulty to estimate it from the four satellite measurements.

Figure 4 shows the comparison between the ideal electron frozen-in term ($\mathbf{E} + \mathbf{v}_e \times \mathbf{B}$) and the ideal ion frozen-in plus the Hall term computed from curlometer ($\mathbf{E} + \mathbf{v}_i \times \mathbf{B} - \mathbf{J}_{curl} \times \mathbf{B}/(en)$). One can see that electrons are mostly magnetized as the ideal frozen-in term does not exceed $1.7 - 2$ mV/m, which is the order of the error bar of the E' measurement (see Sec. VI for details about the error bars). However, at the DF, this term is very close to or exceeds the error bar. This suggests that electrons could be decoupled from the magnetic field. It is difficult to confirm that this decoupling is due to the larger pressure gradient at DF since the calculation of the divergence of the electron pressure tensor is very noisy for such low density plasma conditions.[21,22]

However, single satellite methods can be applied to estimate the possible effect of the electron pressure gradient term at the DF.[14,21] Using the DF velocity obtained from the timing analysis, one can consider that the time variations of the pressure in the spacecraft frame along the normal direction are mostly due to the normal pressure gradient: $\partial P_e/\partial t \sim V_{DF}\partial P_e/\partial N$. Figures 3(c) and 4(c) show this calculation (green line) based on four spacecraft averaged quantities. These figures confirm that the electron pressure gradient term is small but not negligible compared to the ideal frozen-in and Hall field terms. Note that for DF2a and DF2b (respectively, DF3a and DF3b), we have used the smallest estimated V_N. Therefore, the gradient term is overestimated for the fastest DFs (see Table II). At the vicinity of the DF crossing and along the normal direction, this raw estimate allows us to suggest that the departure between the ion frozen-in term and the Hall field (3C) and the non-zero electron frozen-in term (4C) are caused by the electron pressure gradient.

VI. ENERGY CONVERSION PROCESS AT THE DF

The energy conversion processes can be studied by computing the $\mathbf{j} \cdot \mathbf{E}$ term present in the electromagnetic energy conservation equation.[50] The $\mathbf{j} \cdot \mathbf{E}$ term governs the exchanges between electromagnetic and kinetic (thermal and bulk flow) energies in the laboratory or spacecraft frames. Positive values correspond to a load, whereas negative values correspond to a generator.[20,36,50] Figure 5 shows the magnetic and the electric field components, and the current density components computed from particle measurements and the corresponding $\mathbf{j} \cdot \mathbf{E}$ term for each DF event. For all DF events, the DF is associated with a positive $\mathbf{j} \cdot \mathbf{E}$ slightly ahead or at the DF, therefore, to an energy transfer from fields to the plasma (dissipation) in the spacecraft frame. However, a negative value with an equivalent amplitude is measured immediately behind the front, indicating an energy transfer from the plasma to the electromagnetic field. When we calculate separately the three terms of the scalar product using the LMN coordinates, we can see that the main contribution comes from the cross-tail current and electric field components ($J_M \cdot E_M$, not shown). Furthermore, the negative part of the energy conversion term is mostly due to the local reversal of the J_M component while E_M related to the flow motion remains positive. Note that the large variations of E_N at the DF do not lead to any energy conversion as they correspond to the Hall field, therefore, which are perpendicular to the current. Regardless of the sign, energy conversion values range from -0.02 to $+0.02$ nW/m^3 except for a maximum negative value of -0.04 for DF1. Finally, one can notice that the possible flux rope signatures are associated with positive or negative energy conversion terms comparable to those associated with the DF.

The measurement of the energy conversion for a two fluid plasma quantified by $\mathbf{j} \cdot \mathbf{E}'$ (where $\mathbf{E}'$ is the electric field in the ion or electron fluid frames) must be the same in the electron frame ($\mathbf{j} \cdot (\mathbf{E} + \mathbf{v}_e \times \mathbf{B})$) and in the ion frame ($\mathbf{j} \cdot (\mathbf{E} + \mathbf{v}_i \times \mathbf{B})$). The energy conversion process does not depend on the specific fluid frame. Furthermore, it is also mathematically constrained as $\mathbf{j} \cdot (\mathbf{E} + \mathbf{v}_i \times \mathbf{B}) - \mathbf{j} \cdot (\mathbf{E} + \mathbf{v}_e \times \mathbf{B}) = \mathbf{j} \cdot (\mathbf{j}/(en) \times \mathbf{B}) = 0$.[21,33] Hence, this equality can also serve as a cross check of the reliability of our calculation of the energy conversion term $\mathbf{j} \cdot \mathbf{E}'$.

For each DF, Figs. 6(a) and 6(b) display four spacecraft averaged values of $[\mathbf{j} \cdot (\mathbf{E} + \mathbf{v}_e \times \mathbf{B})]$ and $[\mathbf{j} \cdot (\mathbf{E} + \mathbf{v}_i \times \mathbf{B})]$ using the current density estimated from the curlometer and from the particle measurements. We can, therefore, verify that the energy conversion term is equal in the ion and electron frames, attesting to the reliability of the energy conversion term calculation. In the fluid frames, the four spacecraft average of the energy conversion term is mostly negative (from -0.02 to -0.01 nW/m^3) just ahead of the DF and corresponds to an energy transfer from the plasma to the electromagnetic fields (generator or wave radiation) in accordance with a previous MMS single event study.[21] One can notice that, when the curlometer is used, some discrepancies between calculations in ion and electron frames can be seen for DF4. This is due to the fact that some of the current density components are smaller or close to their error bars [e.g., J_N in Fig. 2(c) for DF4] as mentioned in Sec. IV.

For each DF event, Fig. 6(c) shows the energy conversion term for each individual satellite in electron frames. These single satellite calculations indicate that the energy conversion process is not homogeneous at the scale of the tetrahedron (electron scales). Indeed, strong variations of the sign and the amplitude of the energy conversion term are seen from one satellite to another. Such variations suggest that a physical process is going on at the electron scales while the DF is propagating earthward.

For a better understanding of the origin of the non-homogeneity of the energy conversion at the electron scales, we estimated the standard deviation for each component of the current density and the
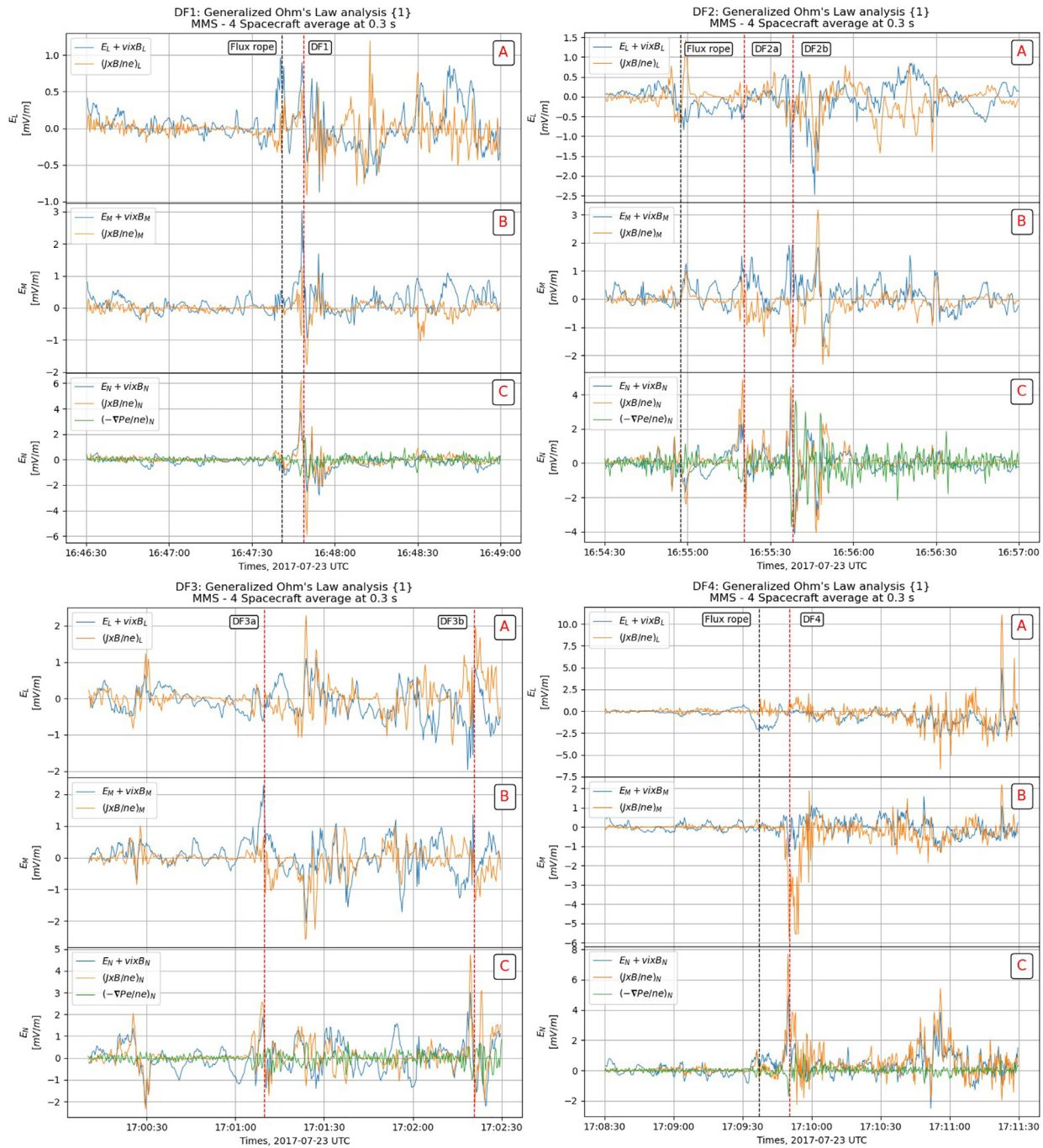
FIG. 3. Panels (a)–(c) show *L*, *M*, *N* components of Ohm's Law terms, respectively: $\mathbf{E} + \mathbf{v_i} \times \mathbf{B}$ (blue line), $(\mathbf{J}_{part} \times \mathbf{B})/(ne)$ (orange line). Panel (c) also includes electron pressure gradient term along *N* (green line).

electric field in the fluid frame ($\mathbf{E}' = \mathbf{E} + \mathbf{v}_e \times \mathbf{B}$) normalized by their respective error bar: $SD(X)/\Delta X = \sqrt{\Sigma_{i=1}^{4}(X_i - \langle X \rangle)^2/4}/\Delta X$, $\langle X \rangle$ being the four spacecraft average of the X component and ΔX its respective estimated error bar. For the electric field, we use the error bar provided by the EDP team ($\sim$1 mV/m),[39] whereas for the electron convective term, the error is estimated as $(\Delta V_e B + V_e \Delta B)$ with $\Delta B = 0.1$ nT[37] and using the moment error bars provided by the FPI
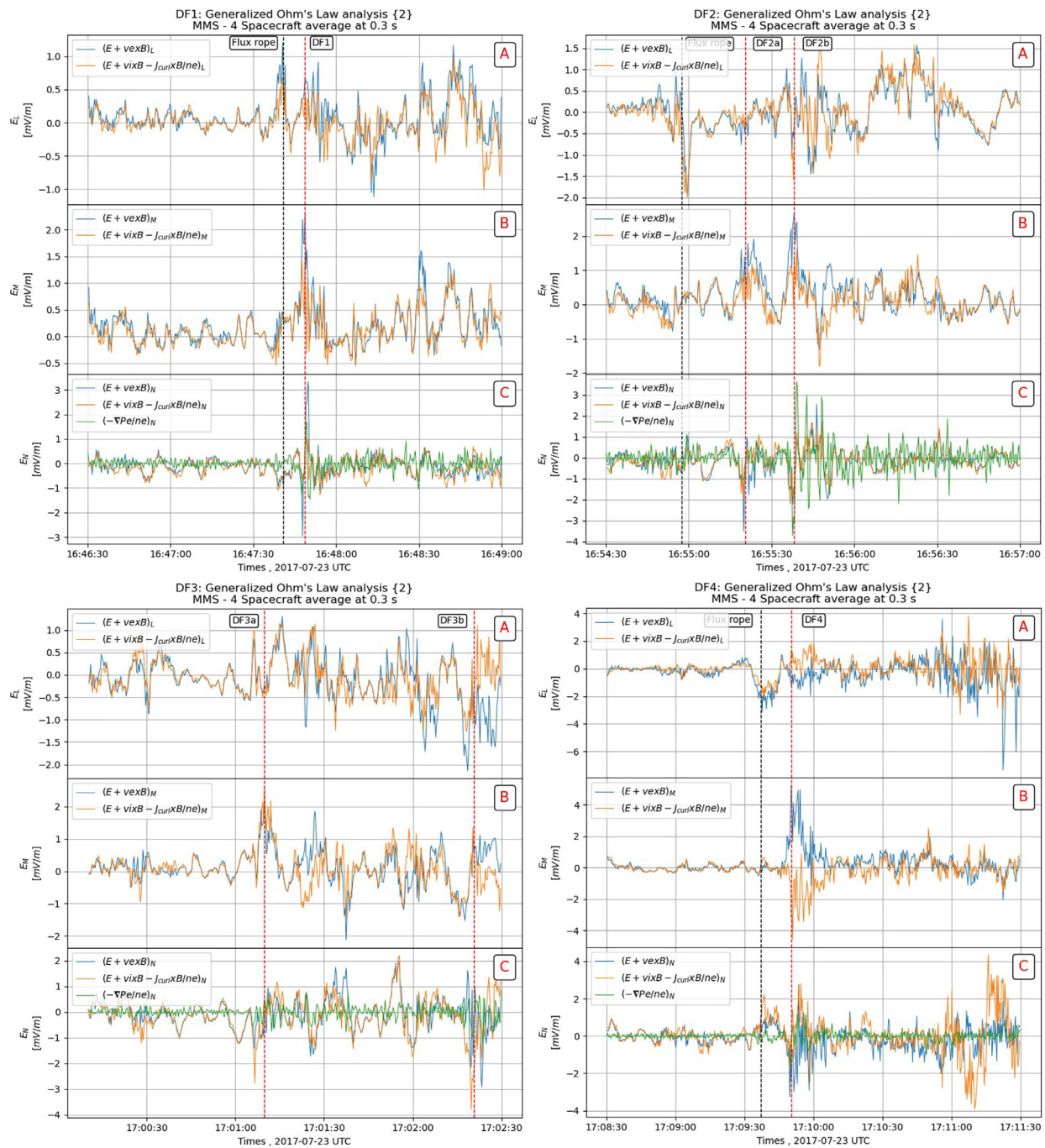
FIG. 4. Panels (a)–(c) show L, M, N components of Ohm's Law terms, respectively: $\mathbf{E} + \mathbf{v_e} \times \mathbf{B}$ (blue line), and $\mathbf{E} + \mathbf{v_i} \times \mathbf{B} - (\mathbf{J}_{curl} \times \mathbf{B})/(ne)$ (orange line). Panel (c) also includes electron pressure gradient term along N (green line).

team.[41] Thus, we found that the error bar of E' averaged over each DF period is $\sim 1.7 - 2$ mV/m. For the error bar of the current density $\Delta J_{part} = e \cdot (\Delta N_e) \cdot (V_i - V_e) + e \cdot N_e \cdot (\Delta V_i + \Delta V_e)$, we got an average value ~ 8 nA/m^2. Let us remember that in the present study,

we use the partial moments, which allow us to deal with smaller errors.

Figures 7(a)–7(c) and 8(a)–8(c) show for each DF, the three components of the current density and the electric field ($\mathbf{E}'$), respectively.
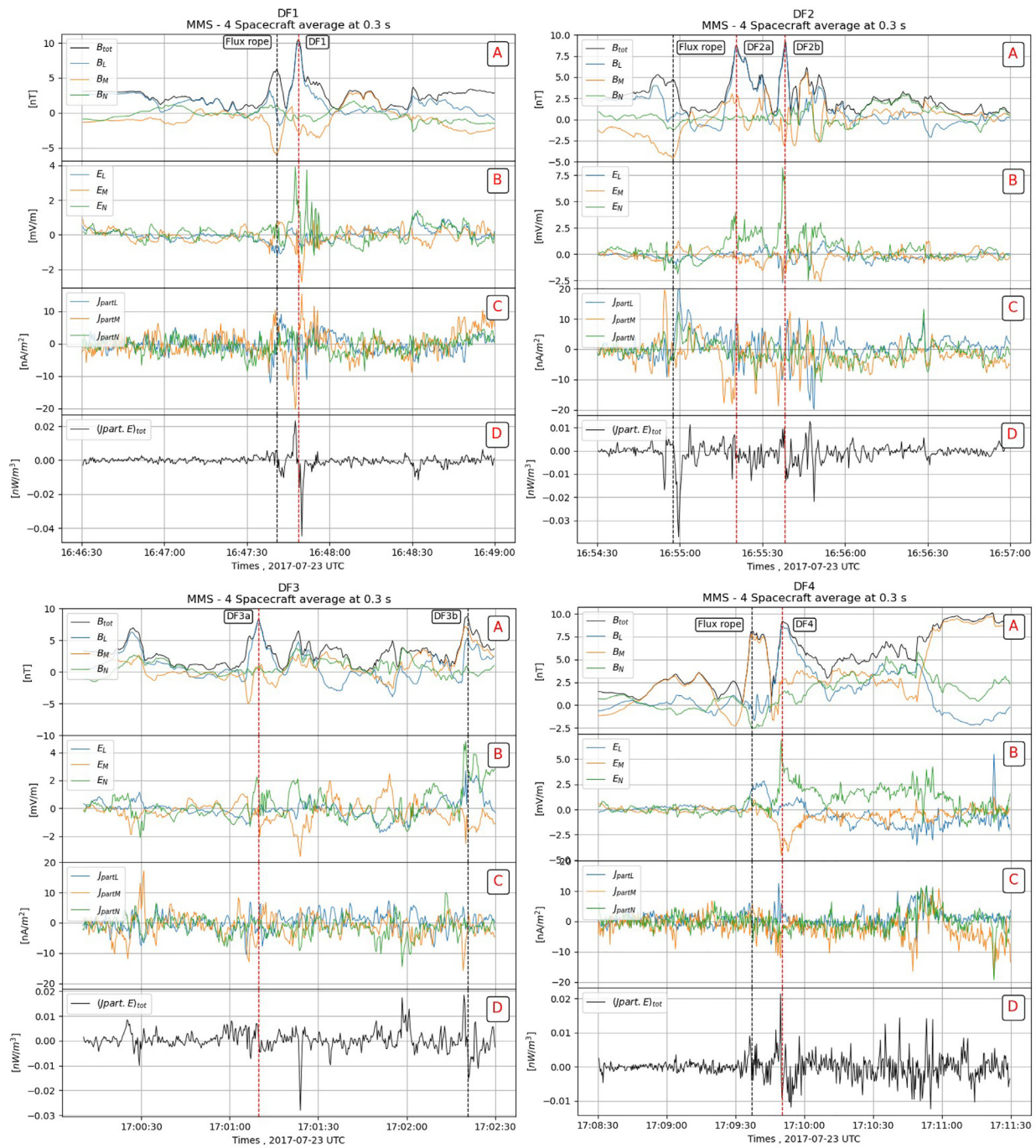
FIG. 5. For each DF event and in LMN frame: (a) magnitude and components of the magnetic field, (b) electric field components, (c) current density components using $\mathbf{J}_{part}$, and (d) energy conversion $\mathbf{j}_{part} \cdot \mathbf{E}$ (in the spacecraft frame).

Figures 7(d), 7(e), 8(d), and 8(e) show the raw and normalized SD of the corresponding quantity. One can see that at DFs, the normalized SD of the electric field ($\mathbf{E}'$) is usually greater (≥ 1) than the normalized SD of the current density (< 1). These results are consistent with the fact that the dispersion between the four curves measured by the four satellites is usually smaller for the current density than for the electric field ($\mathbf{E}'$) [Figs. 7(a)–7(c) and 8(a)–8(c)]. Therefore, the non-homogeneity of the energy conversion process seems to be caused
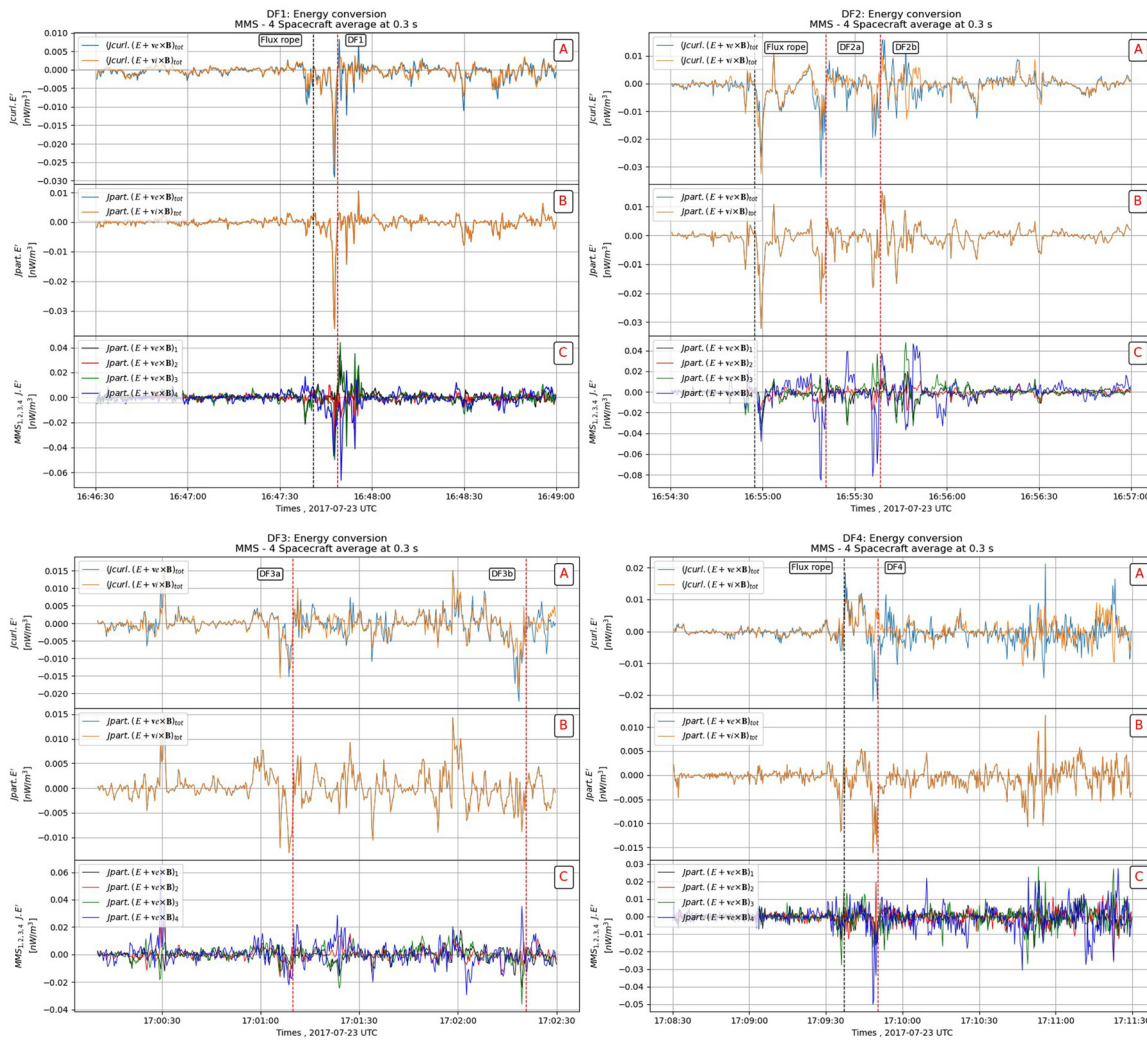
FIG. 6. Comparison of the energy conversion term in both electron and ion frames. (a) Four spacecraft average of the energy conversion using $\mathbf{J}_{curl}$. (b) Four spacecraft average of the energy conversion using $\mathbf{J}_{part}$. (c) Energy conversion using $\mathbf{J}_{part}$ for MMS1 (black), MMS2 (red), MMS3 (green), and MMS4 (blue).

mainly by the electric fluctuations having electron scales. Conversely, the current density remains more homogeneous at the scale of the MMS tetrahedron, which suggests that the origin of the electric field fluctuations is mostly electrostatic as we will discuss in Sec. VII.

VII. DISCUSSION AND SUMMARY

Six DF events embedded in fast earthward flows and detected during a large scale substorm event have been analyzed in the present study. These DF events belong to the most common category corresponding to a decrease in the density and an increase in the temperature;[12] therefore, they are characterized by a transition between a cold dense plasma at rest to a hot tenuous accelerated plasma moving earthward. We analyzed each front orientation using the MVAB method as well as a timing analysis and found that all DFs are mostly moving earthward with some DFs having a significant duskward and

southward motions. We have pointed out that the HPCA V_N velocity is always much larger than FPI V_N, confirming that FPI instrument underestimates the velocity of the earthward flow in the magnetotail due to its low upper energy. This caveat is quite common during substorm events as the plasma is energized due to the global magnetotail reconfiguration. Moreover, the maximum of the V_N component of the ion velocity is always located behind the DF associated with the maximum of B_L, which, according to a statistical study based on Cluster data, should correspond to decelerated DFs with a significant part of the energy being radiated (in the spacecraft frame).[19,47] In order to have more confidence on the particle moment measurements, we have compared the current densities obtained from the particle instruments (using partial moment for electrons) with those obtained from the curlometer technique. Despite relatively small values (<20 nA/m^2) associated with the DF crossing, we found a good agreement between
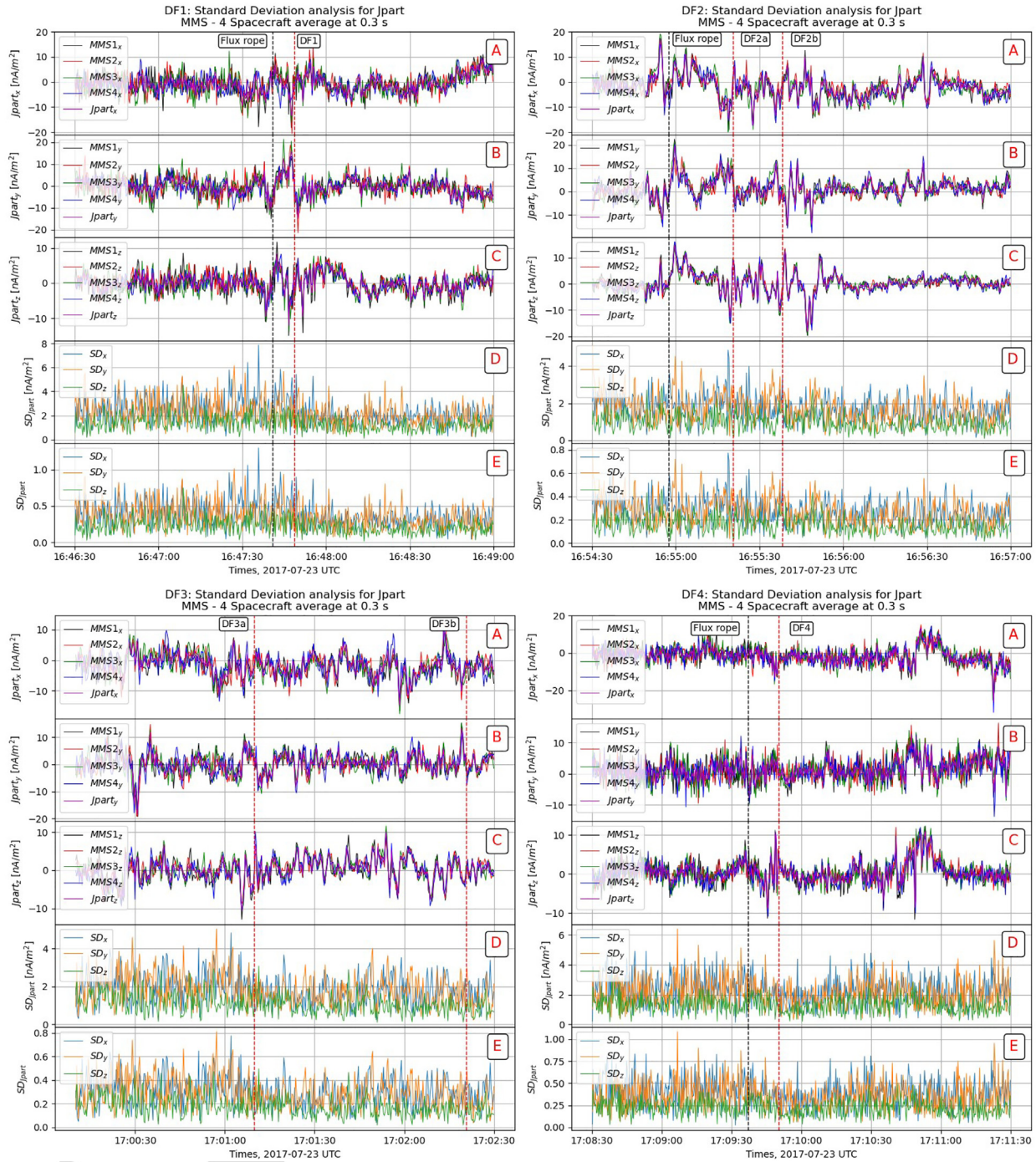
FIG. 7. Components of the current density obtained from FPI in GSE for each MMS satellite and the four spacecraft average [panels (a)–(c)]. Panel D shows the standard deviation SD(j) of each component of the current density. Panel E shows the SD(j) normalized by the current density error bar, see text for details.

the two types of current density estimates. Then, to better understand ion and electron dynamics at the DF crossing, we analyzed Ohm's law. Near the DF crossing, we found that ions are decoupled from the magnetic field due to the Hall field. A clear bipolar signature of the Hall field is present normal to the DF (along N) mostly related to a reversal of the cross-tail current just behind the DF. However, the Hall field does not seem to be sufficient to explain the full decoupling of the ions. The electron pressure gradient term is also likely involved in this
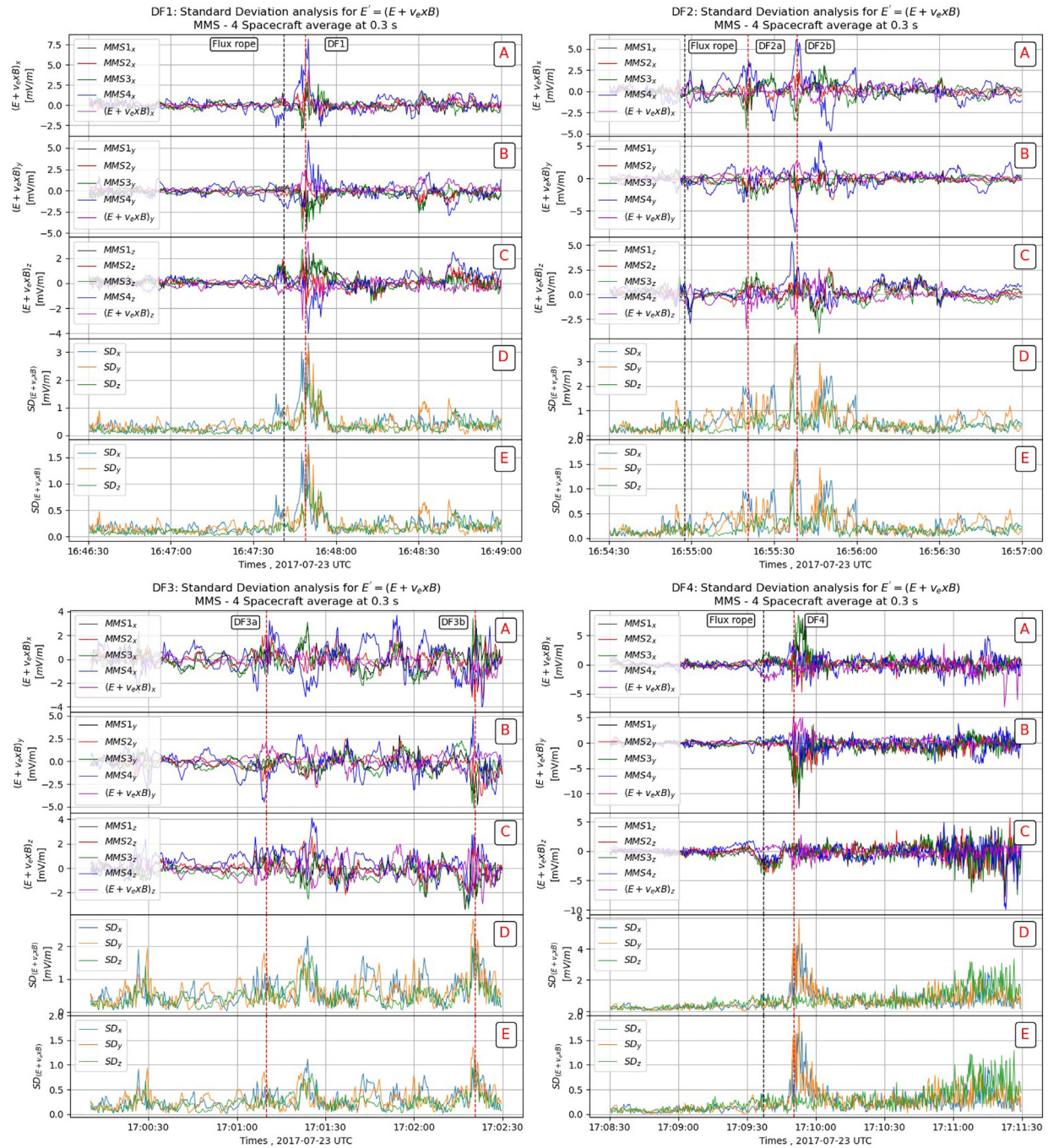
FIG. 8. Same as Fig. 7 for the electric field in the electron frame ($\mathbf{E}' = \mathbf{E} + \mathbf{V}_e \times \mathbf{B}$). Panel E shows the standard deviation normalized by the error bar of $\mathbf{E}'$, see text for details.

decoupling. Due to the low plasma density, we could not compute the divergence of the electron pressure tensor with a sufficient reliability. Instead, we used single satellite method (applied to the four spacecraft averaged data) to estimate the electron pressure gradient along the normal direction.[14,21] For most of the DF events, we found that the signature of the electron pressure gradient along the normal is consistent with a significant contribution to the ion decoupling and could account for the departure between the ideal ion frozen-in term

523 $(\mathbf{E} + \mathbf{v}_i \times \mathbf{B})$ and the Hall field. Electrons are magnetized most of the
524 time. However, at the DF crossing, the departure between the electron
525 ideal frozen-in term $(\mathbf{E} + \mathbf{v_e} \times \mathbf{B})$ is very close to or exceeds the error
526 bar, which also suggests, as for the ions, that the electron pressure
527 term along the normal can take part in the electron decoupling. In the
528 other directions (L and M), it is not possible to estimate the gradient
529 by the same technique. However, the results obtained along the nor-
530 mal suggest that the decoupling along L and M also involves the elec-
531 tron pressure term in these directions.

532   In order to investigate the energy conversion process at the DF,
533 we have estimated the $\mathbf{j} \cdot \mathbf{E}$ term.[17,19–22,26,51] For all DFs in the space-
534 craft frame, we found that the energy is transferred from the electro-
535 magnetic field to the plasma (dissipation or loading) at or just ahead
536 of the DF and from the plasma to the electromagnetic field behind the
537 DF (wave radiation or generator). The amplitudes of the positive and
538 negative peaks have similar values (± 0.02 nW·m^{-3}), which do not
539 allow us to draw conclusions about a net energy transfer between fields
540 and particles, despite the fact that the normal velocity peak is detected
541 behind the front.[19,47] This reversal of the energy conversion is mostly
542 related to the reversal of the cross-tail current component (J_M) just
543 behind the front. Such a current reversal at the DF has been already
544 mentioned by Yao *et al.* based on 2003 Cluster data (subproton scale
545 spacecraft separation $\sim$200 km) but only related to DFs preceded by a
546 dip of the magnetic field.[46] It has been also recently mentioned by Liu
547 *et al.* in a previous MMS single DF case study event leading to a nega-
548 tive $\mathbf{j} \cdot \mathbf{E}$ behind the DF. The origin of this reversal is not fully under-
549 stood and could be due to a current density shear at an electron scale
550 between the main front and the front trailing part. Another possibility
551 could be the formation of substructures, such as electron vortices
552 driven by the current carried by electrons within the front region,
553 which could contribute locally to the increase in the total magnetic
554 field.[52] The existence of such structures within the ion scale DF struc-
555 ture needs to be confirmed by further studies. Whatever the origin of
556 these current density reversals, these results suggest that DFs have
557 complex substructures that make difficult to draw conclusions about
558 the net energy transfer in the spacecraft frame.

559   To better understand this energy conversion process, we have
560 carried out the computation in each fluid frame (ion and electron)
561 using four spacecraft average value of $\mathbf{E}'$ and $\mathbf{j}$. Egality of the calcula-
562 tion in both ion and electron frames has been used as a reliability test.
563 In these fluid frames, the $\mathbf{j} \cdot \mathbf{E}'$ just ahead of the DF is negative most of
564 the time indicating a net transfer from the plasma to the electromag-
565 netic fields as also found in a previous MMS single DF event.[21]
566 Therefore, the energy would be radiated and this process should lead
567 to the deceleration of the fast plasma flow. Note that this negative
568 term cannot be related to the electron pressure gradient along the nor-
569 mal since this latter is perpendicular to the main current J_M. However,
570 as we mentioned in Sec. V, the electron decoupling along M can also
571 be due to the electron pressure gradient along this direction and leads
572 to negative $\mathbf{j} \cdot \mathbf{E}' \sim J_M.E'_M = -J_M.|\nabla P_e|_M/(en)$.

573   Furthermore, we have analyzed the homogeneity of this energy
574 conversion process by computing the $\mathbf{j} \cdot \mathbf{E}'$ term for each satellite. We
575 found that the energy conversion is not homogeneous at the scale of
576 the tetrahedron, i.e., at the electron scales. By computing the standard
577 deviation of $\mathbf{E}'$ and $\mathbf{j}$ normalized by their respective error bars, we
578 showed that the non-homogeneity of the energy conversion process
579 comes mostly from the electric field fluctuations while the

580 contribution of current density fluctuations is smaller. As mentioned
581 above, these electric field fluctuations should be related to the electron
582 pressure gradient. This result is consistent with previous studies, which
583 identified large amplitude electric field fluctuations related to lower-
584 hybrid drift waves from space observations.[22–26] It is also consistent
585 with 3D PIC simulations.[30,33,34] These waves with frequencies between
586 ion and electron gyrofrequencies ($f_{ci} < f < f_{ce}$) are expected to be gen-
587 erated by the large density gradient ($n_e/\nabla n_e \sim c/\omega_{pi}$) at DF and are
588 known to have wavelengths on the order of the electron Larmor radius
589 for the fastest growing mode.[53,54] These electron-scale wavelengths
590 correspond to the average spacecraft separation for these events, and
591 the period of the LHD waves is much smaller than the DF crossing
592 time. These waves are able to generate ripples on the front at the
593 electron scales, which can lead to the non-homogeneity of the energy
594 conversion process.[27] Indeed, these waves are considered as "quasi-
595 electrostatic" waves. Due to their frequency range, ions can be
596 assumed unmagnetized, whereas electrons are magnetized.[54]
597 Therefore, electron drift in the electric field of the waves produces
598 small perpendicular (to the background magnetic field) currents and a
599 parallel magnetic field perturbations causing the ripple of the front at
600 electron scales. These currents are much smaller than the current asso-
601 ciated with the front. Thus, regarding the energy conversion process in
602 the fluid frame ($\mathbf{J} \cdot \mathbf{E}'$), the dominant term corresponds to the product
603 between the ion-scale current associated with the front ($\mathbf{J}_0$) and the
604 electron-scale electric field associated with the LHD waves ($\boldsymbol{\delta E}'$). The
605 energy conversion ($\boldsymbol{\delta J} \cdot \boldsymbol{\delta E}'$) due to currents generated by LHD waves
606 ($\boldsymbol{\delta J}$) is smaller and can be considered as a second order contribution
607 compared to the former term. This can be summarized as $\mathbf{J} \cdot \mathbf{E}'$
608 $\simeq \mathbf{J}_0 \cdot \boldsymbol{\delta E}'$ with $\boldsymbol{\delta J} \cdot \boldsymbol{\delta E}' \ll \mathbf{J}_0 \cdot \boldsymbol{\delta E}'$. The non-linear evolution of these
609 waves could generate electron scale vortices[55] that could explain the
610 current density reversal behind the DF and the negative part of $\mathbf{j} \cdot \mathbf{E}$
611 although the low inhomogeneity of the current density at the scale of
612 the tetrahedron is not in favor of this interpretation.

613   However, from their 3D PIC simulations, Nakamura *et al.* found
614 an oscillating $\mathbf{j} \cdot \mathbf{E}'$, which once integrated along the cross-tail direction
615 leads to a non-zero positive term corresponding to an energy dissipa-
616 tion.[34] The detailed characterization of the wave activity associated
617 with these DF is beyond the scope of the present study and left for a
618 further investigation. However, our results support the fact that the
619 non-homogeneity of the energy conversion process at the electron
620 scales is likely due to the electric field fluctuations of the lower-hybrid
621 drift instability that develops in the vicinity of the DF due to the large
622 density gradient; this density gradient being due to a combined effect
623 of the tangential nature of the DF and the propagation of a tenuous
624 (and hot) plasma through a denser (and colder) plasma at rest. The
625 present study also confirms the need for a three-dimensional analysis
626 of the energy conversion process at the DF as the lower-hybrid drift
627 waves causing the electron scale variations of the front propagate in
628 the direction perpendicular to density gradient, therefore, perpendicu-
629 lar to the direction of the fast plasma flow.[24,26] The net energy transfer
630 at DF needs not only to be investigated and integrated along the direc-
631 tion of the plasma flow but also perpendicularly to the DF density gra-
632 dient. Therefore, the role of DF in the global energy cycle of the
633 Earth's magnetosphere still needs further investigation and in particu-
634 lar statistical studies focused on the energy conversion process at DF
635 need to take into account these electron scale substructures. Indeed,
636 the positive than negative $\mathbf{J} \cdot \mathbf{E}$ terms at and behind the DF,

respectively, confirm that DFs play an important role in this cycle. Their contribution is not only related to a local dissipative effect (at DF) but also to the generation of electromagnetic fields (just behind the DF). This latter contribution can be (i) associated with the emission of waves that can transport energy to other regions (e.g., auroral region) and interact with the particles causing their acceleration or (ii) associated with the formation of coherent electromagnetic structures, such as kinetic-scale vortices that can contribute to and modify the energy and plasma transport.[58,59]

ACKNOWLEDGMENTS

AUTHOR DECLARATIONS

Conflict of Interest

The authors have no conflicts to disclose.

DATA AVAILABILITY

The MMS data that support the findings of this study are publicly available from the MMS Science Data Center (http://lasp.colorado.edu/mms/sdc/public/), Ref. 57.

REFERENCES

[1]W. Baumjohann, G. Paschmann, and H. Luehr, "Characteristics of high-speed ion flows in the plasma sheet," J. Geophys. Res.: Space Phys. **95**, 3801–3809, https://doi.org/10.1029/JA095iA04p03801 (1990).

[2]V. Angelopoulos, W. Baumjohann, C. F. Kennel, F. V. Coronti, M. G. Kivelson, R. Pellat, R. J. Walker, H. Luehr, and G. Paschmann, "Bursty bulk flows in the inner central plasma sheet," J. Geophys. Res.: Space Phys. **97**, 4027–4039, https://doi.org/10.1029/91JA02701 (1992).

[3]K. Shiokawa, W. Baumjohann, and G. Haerendel, "Braking of high-speed flows in the near-Earth tail," Geophys. Res. Lett. **24**, 1179–1182, https://doi.org/10.1029/97GL01062 (1997).

[4]K. Shiokawa, W. Baumjohann, G. Haerendel, G. Paschmann, J. F. Fennell, E. Friis-Christensen, H. Lühr, G. D. Reeves, C. T. Russell, P. R. Sutcliffe, and K. Takahashi, "High-speed ion flow, substorm current wedge, and multiple Pi 2 pulsations," J. Geophys. Res.: Space Phys. **103**, 4491–4508, https://doi.org/10.1029/97JA01680 (1998).

[5]M. I. Sitnov, M. Swisdak, and A. V. Divin, "Dipolarization fronts as a signature of transient reconnection in the magnetotail," J. Geophys. Res.: Space Phys. **114**, A04202 (2009).

[6]J. F. Drake, M. Swisdak, P. A. Cassak, and T. D. Phan, "On the 3-D structure and dissipation of reconnection-driven flow bursts," Geophys. Res. Lett. **41**, 3710–3716, https://doi.org/10.1002/2014GL060249 (2014).

[7]H. S. Fu, J. B. Cao, Y. V. Khotyaintsev, M. I. Sitnov, A. Runov, S. Y. Fu, M. Hamrin, M. André, A. Retinò, Y. D. Ma, H. Y. Lu, X. H. Wei, and S. Y. Huang, "Dipolarization fronts as a consequence of transient reconnection: In situ evidence," Geophys. Res. Lett. **40**, 6023–6027, https://doi.org/10.1002/2013GL058620 (2013).

[8]P. L. Pritchett and F. V. Coroniti, "A kinetic ballooning/interchange instability in the magnetotail," J. Geophys. Res.: Space Phys. **115**, A06301 (2010).

[9]D. H. Pontius, Jr. and R. A. Wolf, "Transient flux tubes in the terrestrial magnetosphere," Geophys. Res. Lett. **17**, 49–52, https://doi.org/10.1029/GL017i001p00049 (1990).

[10]S.-I. Ohtani, M. A. Shay, and T. Mukai, "Temporal structure of the fast convective flow in the plasma sheet: Comparison between observations and two-fluid simulations," J. Geophys. Res.: Space Phys. **109**, A03210 (2004).

[11]A. Runov, V. Angelopoulos, M. I. Sitnov, V. A. Sergeev, J. Bonnell, J. P. McFadden, D. Larson, K.-H. Glassmeier, and U. Auster, "THEMIS observations of an earthward-propagating dipolarization front," Geophys. Res. Lett. **36**, L14106, https://doi.org/10.1029/2009GL038980 (2009).

[12]D. Schmid, R. Nakamura, F. Plaschke, M. Volwerk, and W. Baumjohann, "Two states of magnetotail dipolarization fronts: A statistical study," J. Geophys. Res.: Space Phys. **120**, 1096–1108, https://doi.org/10.1002/2014JA020380 (2015).

[13]J. Liu, V. Angelopoulos, A. Runov, and X.-Z. Zhou, "On the current sheets surrounding dipolarizing flux bundles in the magnetotail: The case for wedgelets," J. Geophys. Res.: Space Phys. **118**, 2000–2020, https://doi.org/10.1002/jgra.50092 (2013).

[14]H. S. Fu, Y. V. Khotyaintsev, A. Vaivads, M. André, and S. Y. Huang, "Electric structure of dipolarization front at sub-proton scale," Geophys. Res. Lett. **39**, L06105, https://doi.org/10.1029/2012GL051274 (2012).

[15]Y. V. Khotyaintsev, C. M. Cully, A. Vaivads, M. André, and C. J. Owen, "Plasma jet braking: energy dissipation and nonadiabatic electrons," Phys. Rev. Lett. **106**, 165001 (2011).

[16]H. Fu, E. E. Grigorenko, C. Gabrielse, C. Liu, S. Lu, K. J. Hwang, X. Zhou, Z. Wang, and F. Chen, "Magnetotail dipolarization fronts and particle acceleration: A review," Sci. China Earth Sci. **63**, 235–256 (2020).

[17]V. Angelopoulos, A. Runov, X. Z. Zhou, D. L. Turner, S. A. Kiehas, S. S. Li, and I. Shinohara, "Electromagnetic energy conversion at reconnection fronts," Science **341**, 1478–1482 (2013).

[18]C. C. Chaston, J. W. Bonnell, L. Clausen, and V. Angelopoulos, "Energy transport by kinetic-scale electromagnetic waves in fast plasma sheet flows," J. Geophys. Res.: Space Phys. **117**, A09202 (2012).

[19]M. Hamrin, T. Pitkänen, P. Norqvist, T. Karlsson, H. Nilsson, M. André, S. Buchert, A. Vaivads, O. Marghitu, B. Klecker, L. M. Kistler, and I. Dandouras, "Evidence for the braking of flow bursts as they propagate toward the Earth," J. Geophys. Res.: Space Phys. **119**, 9004–9018, https://doi.org/10.1002/2014JA020285 (2014).

[20]S. Y. Huang, H. S. Fu, Z. G. Yuan, M. Zhou, S. Fu, X. H. Deng, W. J. Sun, Y. Pang, D. D. Wang, H. M. Li, H. M. Li, and X. D. Yu, "Electromagnetic energy conversion at dipolarization fronts: Multispacecraft results," J. Geophys. Res.: Space Phys. **120**, 4496–4502, https://doi.org/10.1002/2015JA021083 (2015).

[21]Z. H. Yao, I. J. Rae, R. L. Guo, A. N. Fazakerley, C. J. Owen, R. Nakamura, W. Baumjohann, C. E. J. Watt, K. J. Hwang, B. L. Giles, C. T. Russell, R. B. Torbert, A. Varsani, H. S. Fu, Q. Q. Shi, and X. J. Zhang, "A direct examination of the dynamics of dipolarization fronts using MMS," J. Geophys. Res.: Space Phys. **122**, 4335–4347, https://doi.org/10.1002/2016JA023401 (2017).

[22]C. M. Liu, H. S. Fu, Y. Xu, Y. V. Khotyaintsev, J. L. Burch, R. E. Ergun, D. G. Gershman, and R. B. Torbert, "Electron-scale measurements of dipolarization front," Geophys. Res. Lett. **45**, 4628–4638, https://doi.org/10.1029/2018GL077928 (2018).

[23]V. Sergeev, V. Angelopoulos, S. Apatenkov, J. Bonnell, R. Ergun, R. Nakamura, J. McFadden, D. Larson, and A. Runov, "Kinetic structure of the sharp injection/dipolarization front in the flow-braking region," Geophys. Res. Lett. **36**, L21105, https://doi.org/10.1029/2009GL040658 (2009).

[24]A. Divin, Y. V. Khotyaintsev, A. Vaivads, and M. André, "Lower hybrid drift instability at a dipolarization front," J. Geophys. Res.: Space Phys. **120**, 1124–1132, https://doi.org/10.1002/2014JA020528 (2015).

[25]O. Le Contel, R. Nakamura, H. Breuillard, M. R. Argall, D. B. Graham, D. Fischer, A. Retinò, M. Berthomier, R. Pottelette, L. Mirioni, T. Chust, F. D. Wilder, D. J. Gershman, A. Varsani, P. A. Lindqvist, Y. V. Khotyaintsev, C. Norgren, R. E. Ergun, K. A. Goodrich, J. L. Burch, R. B. Torbert, J. Needell, M. Chutter, D. Rau, I. Dors, C. T. Russell, W. Magnes, R. J. Strangeway, K. R. Bromund, H. Y. Wei, F. Plaschke, B. J. Anderson, G. Le, T. E. Moore, B. L. Giles, W. R. Paterson, C. J. Pollock, J. C. Dorelli, L. A. Avanov, Y. Saito, B. Lavraud, S. A. Fuselier, B. H. Mauk, I. J. Cohen, D. L. Turner, J. F. Fennell, T. Leonard, and A. N. Jaynes, "Lower hybrid drift waves and electromagnetic electron space-phase holes associated with dipolarization fronts and field-aligned currents observed by the magnetospheric multiscale mission during a substorm," J. Geophys. Res.: Space Phys. **122**, 12236–12257, https://doi.org/10.1002/2017JA024550 (2017).

26. J. Yang, J. B. Cao, H. S. Fu, T. Y. Wang, W. L. Liu, and Z. H. Yao, "Broadband high-frequency waves detected at dipolarization fronts," J. Geophys. Res.: Space Phys. **122**, 4299–4307, https://doi.org/10.1002/2016JA023465 (2017).

27. D.-X. Pan, Y. V. Khotyaintsev, D. B. Graham, A. Vaivads, X.-Z. Zhou, M. André, P.-A. Lindqvist, R. E. Ergun, O. Le Contel, C. T. Russell, R. B. Torbert, B. Giles, and J. L. Burch, "Rippled electron-scale structure of a dipolarization front," Geophys. Res. Lett. **45**, 12,116–12,124, https://doi.org/10.1029/2018GL080826 (2018).

28. Z. H. Zhong, X. H. Deng, M. Zhou, W. Q. Ma, R. X. Tang, Y. V. Khotyaintsev, B. L. Giles, C. T. Russell, and J. L. Burch, "Energy conversion and dissipation at dipolarization fronts: A statistical overview," Geophys. Res. Lett. **46**, 12,693–12,701, https://doi.org/10.1029/2019GL085409 (2019).

29. L. Q. Zhang, W. Baumjohann, Y. V. Khotyaintsev, J. L. Burch, J. Webster, J. Y. Wang, C. Wang, L. Dai, and C. Y. Zhang, "BBF deceleration down-tail of $X < -15 R_E$ From MMS Observation," J. Geophys. Res.: Space Phys. **125**, e26837 (2020).

30. A. Divin, Y. V. Khotyaintsev, A. Vaivads, M. André, S. Markidis, and G. Lapenta, "Evolution of the lower hybrid drift instability at reconnection jet front," J. Geophys. Res.: Space Phys. **120**, 2675–2690, https://doi.org/10.1002/2014JA020503 (2015).

31. Y. V. Khotyaintsev, A. Divin, A. Vaivads, M. André, and S. Markidis, "Energy conversion at dipolarization fronts," Geophys. Res. Lett. **44**, 1234–1242, https://doi.org/10.1002/2016GL071909 (2017).

32. Y. Yang, W. H. Matthaeus, T. N. Parashar, C. C. Haggerty, V. Roytershteyn, W. Daughton, M. Wan, Y. Shi, and S. Chen, "Energy transfer, pressure tensor, and heating of kinetic plasma," Phys. Plasmas **24**, 072306 (2017).

33. M. I. Sitnov, V. G. Merkin, V. Roytershteyn, and M. Swisdak, "Kinetic dissipation around a dipolarization front," Geophys. Res. Lett. **45**, 4639–4647, https://doi.org/10.1029/2018GL077874 (2018).

34. T. K. M. Nakamura, T. Umeda, R. Nakamura, H. S. Fu, and M. Oka, "Disturbance of the front region of magnetic reconnection outflow jets due to the lower-hybrid drift instability," Phys. Rev. Lett. **123**, 235101 (2019).

35. J. L. Burch, R. B. Torbert, T. D. Phan, L.-J. Chen, T. E. Moore, R. D. Ergun, J. P. Eastwood, D. J. Gershman, P. A. Cassak, M. R. Argall, S. Wang, M. Hesse, C. J. Pollock, B. L. Giles, R. Nakamura, B. H. Mauk, S. A. Fuselier, C. T. Russell, R. J. Strangeway, J. F. Drake, M. A. Shay, Y. V. Khotyaintsev, G. Lindqvist, P.-A. Marklund, F. D. Wilder, D. T. Young, K. Torkar, J. Goldstein, J. C. Dorelli, L. A. Avanov, M. Oka, D. N. Baker, A. N. Jaynes, K. A. Goodrich, I. J. Cohen, D. L. Turner, J. F. Fennell, J. B. Blake, J. Clemmons, M. Goldman, D. Newman, S. M. Petrinec, K. J. Trattner, B. Lavraud, P. H. Reiff, W. Baumjohann, W. Magnes, M. Steller, W. Lewis, Y. Saito, V. Coffey, and M. Chandler, "Electron-scale measurements of magnetic reconnection in space," Science **352**, 1176 (2016).

36. R. B. Torbert, C. T. Russell, W. Magnes, R. E. Ergun, P.-A. Lindqvist, O. LeContel, H. Vaith, J. Macri, S. Myers, D. Rau, J. Needell, B. King, M. Granoff, M. Chutter, I. Dors, G. Olsson, Y. V. Khotyaintsev, A. Eriksson, C. A. Kletzing, S. Bounds, B. Anderson, W. Baumjohann, M. Steller, K. Bromund, G. Le, R. Nakamura, R. J. Strangeway, H. K. Leinweber, S. Tucker, J. Westfall, D. Fischer, F. Plaschke, J. Porter, and K. Lappalainen, "The FIELDS instrument suite on MMS: Scientific objectives, measurements, and data products," Space Sci. Rev. **199**, 105–135 (2016).

37. C. T. Russell, B. J. Anderson, W. Baumjohann, K. R. Bromund, D. Dearborn, D. Fischer, G. Le, H. K. Leinweber, D. Leneman, W. Magnes, J. D. Means, M. B. Moldwin, R. Nakamura, D. Pierce, F. Plaschke, K. M. Rowe, J. A. Slavin, R. J. Strangeway, R. Torbert, C. Hagen, I. Jernej, A. Valavanoglou, and I. Richter, "The Magnetospheric Multiscale Magnetometers," Space Sci. Rev. **199**, 189–256 (2016).

38. R. E. Ergun, S. Tucker, J. Westfall, K. A. Goodrich, D. M. Malaspina, D. Summers, J. Wallace, M. Karlsson, J. Mack, N. Brennan, B. Pyke, P. Withnell, R. Torbert, J. Macri, D. Rau, I. Dors, J. Needell, P.-A. Lindqvist, G. Olsson, and C. M. Cully, "The axial double probe and fields signal processing for the MMS mission," Space Sci. Rev. **199**, 167–188 (2016).

39. P.-A. Lindqvist, G. Olsson, R. B. Torbert, B. King, M. Granoff, D. Rau, G. Needell, S. Turco, I. Dors, P. Beckman, J. Macri, C. Frost, J. Salwen, A. Eriksson, L. Åhlén, Y. V. Khotyaintsev, J. Porter, K. Lappalainen, R. E. Ergun, W. Wermeer, and S. Tucker, "The spin-plane double probe electric field instrument for MMS," Space Sci. Rev. **199**, 137–165 (2016).

40. C. Pollock, T. Moore, A. Jacques, J. Burch, U. Gliese, Y. Saito, T. Omoto, L. Avanov, A. Barrie, V. Coffey, J. Dorelli, D. Gershman, B. Giles, T. Rosnack, C. Salo, S. Yokota, M. Adrian, C. Aoustin, C. Auletti, S. Aung, V. Bigio, N. Cao, M. Chandler, D. Chornay, K. Christian, G. Clark, G. Collinson, T. Corris, A. De Los Santos, R. Devlin, T. Diaz, T. Dickerson, C. Dickson, A. Diekmann, F. Diggs, C. Duncan, A. Figueroa-Vinas, C. Firman, M. Freeman, N. Galassi, K. Garcia, G. Goodhart, D. Guerrero, J. Hageman, J. Hanley, E. Hemminger, M. Holland, M. Hutchins, T. James, W. Jones, S. Kreisler, J. Kujawski, V. Lavu, J. Lobell, E. LeCompte, A. Lukemire, E. MacDonald, A. Mariano, T. Mukai, K. Narayanan, Q. Nguyan, M. Onizuka, W. Paterson, S. Persyn, B. Piepgrass, F. Cheney, A. Rager, T. Raghuram, A. Ramil, L. Reichenthal, H. Rodriguez, J. Rouzaud, A. Rucker, Y. Saito, M. Samara, J.-A. Sauvaud, D. Schuster, M. Shappirio, K. Shelton, D. Sher, D. Smith, K. Smith, S. Smith, D. Steinfeld, R. Szymkiewicz, K. Tanimoto, J. Taylor, C. Tucker, K. Tull, A. Uhl, J. Vloet, P. Walpole, S. Weidner, D. White, G. Winkert, P.-S. Yeh, and M. Zeuch, "Fast Plasma Investigation for Magnetospheric Multiscale," Space Sci. Rev. **199**, 331–406 (2016).

41. D. J. Gershman, J. C. Dorelli, A. F.-Vinas, and C. J. Pollock, "The calculation of moment uncertainties from velocity distribution functions with random errors," J. Geophys. Res.: Space Phys. **120**, 6633–6645, https://doi.org/10.1002/2014JA020775 (2015).

42. D. T. Young, J. L. Burch, R. G. Gomez, A. De Los Santos, G. P. Miller, P. Wilson, N. Paschalidis, S. A. Fuselier, K. Pickens, E. Hertzberg, C. J. Pollock, J. Scherrer, P. B. Wood, E. T. Donald, D. Aaron, J. Furman, D. George, R. S. Gurnee, R. S. Hourani, A. Jacques, T. Johnson, T. Orr, K. S. Pan, S. Persyn, S. Pope, J. Roberts, M. R. Stokes, K. J. Trattner, and J. M. Webster, "Hot plasma composition analyzer for the Magnetospheric Multiscale Mission," Space Sci. Rev. **199**, 407–470 (2016).

43. G. Chanteur and C. Harvey, "Spatial interpolation for four spacecraft: Application to magnetic gradients," in *Analysis Methods for Multi-Spacecraft Data*, ISSI Scientific Report SR-001, edited by G. Paschman and P. Daly (European Space Agency, 1998), Chap. 15, pp. 371–393.

44. B. U. Ö. Sonnerup and M. Scheible, "Minimum and maximum variance analysis," in *ISSI Scientific Reports Series* (■, 1998), Vol. 1, pp. 185–220.

45. H. S. Fu, Y. V. Khotyaintsev, A. Vaivads, M. André, V. A. Sergeev, S. Y. Huang, E. A. Kronberg, and P. W. Daly, "Pitch angle distribution of suprathermal electrons behind dipolarization fronts: A statistical overview," J. Geophys. Res.: Space Phys. **117**, A12221 (2012).

46. Z. Yao, W. J. Sun, S. Y. Fu, Z. Y. Pu, J. Liu, V. Angelopoulos, X. J. Zhang, X. N. Chu, Q. Q. Shi, R. L. Guo, and Q. G. Zong, "Current structures associated with dipolarization fronts," J. Geophys. Res.: Space Phys. **118**, 6980–6985, https://doi.org/10.1002/2013JA019290 (2013).

47. H. S. Fu, Y. V. Khotyaintsev, M. André, and A. Vaivads, "Fermi and betatron acceleration of suprathermal electrons behind dipolarization fronts," Geophys. Res. Lett. **38**, L16104, https://doi.org/10.1029/2011GL048528 (2011).

48. A. T. Y. Lui, Y. Zheng, H. RèMe, M. W. Dunlop, G. Gustafsson, and C. J. Owen, "Breakdown of the frozen-in condition in the Earth's magnetotail," J. Geophys. Res.: Space Phys. **112**, A04215 (2007).

49. R. B. Torbert, J. L. Burch, B. L. Giles, D. Gershman, C. J. Pollock, J. Dorelli, L. Avanov, M. R. Argall, J. Shuster, R. J. Strangeway, C. T. Russell, R. E. Ergun, F. D. Wilder, K. Goodrich, H. A. Faith, C. J. Farrugia, P. A. Lindqvist, T. Phan, Y. Khotyaintsev, T. E. Moore, G. Marklund, W. Daughton, W. Magnes, C. A. Kletzing, and S. Bounds, "Estimates of terms in Ohm's law during an encounter with an electron diffusion region," Geophys. Res. Lett. **43**, 5918–5925, https://doi.org/10.1002/2016GL069553 (2016).

50. J. Birn and M. Hesse, "Energy release and conversion by reconnection in the magnetotail," Ann. Geophys. **23**, 3365–3373 (2005).

51. Y. Xu, H. Fu, J. Cao, C. Liu, C. Norgren, and Z. Chen, "Electron scale measurements of antidipolarization front," Geophys. Res. Lett. **48**, e92232, https://doi.org/10.1029/2020GL092232 (2021).

52. J. E. Stawarz, J. P. Eastwood, K. J. Genestreti, R. Nakamura, R. E. Ergun, D. Burgess, J. L. Burch, S. A. Fuselier, D. J. Gershman, B. L. Giles, O. Le Contel, P. A. Lindqvist, C. T. Russell, and R. B. Torbert, "Intense electric fields and electron-scale substructure within magnetotail flux ropes as revealed by the Magnetospheric Multiscale Mission," Geophys. Res. Lett. **45**, 8783–8792, https://doi.org/10.1029/2018GL079095 (2018).

AQ7

[53] R. C. Davidson and N. T. Gladd, "Anomalous transport properties associated with the lower-hybrid-drift instability," Phys. Fluids **18**, 1327–1335 (1975).

[54] J. D. Huba, N. T. Gladd, and K. Papadopoulos, "Lower-hybrid-drift wave turbulence in the distant magnetotail," J. Geophys. Res.: Space Phys. **83**, 5217–5226, https://doi.org/10.1029/JA083iA11p05217 (1978).

[55] L. J. Chen, S. Wang, O. Le Contel, A. Rager, M. Hesse, J. Drake, J. Dorelli, J. Ng, N. Bessho, D. Graham, L. B. Wilson, T. Moore, B. Giles, W. Paterson, B. Lavraud, K. Genestreti, R. Nakamura, Y. V. Khotyaintsev, R. E. Ergun, R. B. Torbert, J. Burch, C. Pollock, C. T. Russell, P. A. Lindqvist, and L. Avanov, "Lower-hybrid drift waves driving electron nongyrotropic heating and vortical flows in a magnetic reconnection layer," **125**, 025103 (2020).

[56] V. Angelopoulos, P. Cruce, A. Drozdov, E. W. Grimes, N. Hatzigeorgiu, D. A. King, D. Larson, J. W. Lewis, J. M. McTiernan, D. A. Roberts, C. L. Russell, T. Hori, Y. Kasahara, A. Kumamoto, A. Matsuoka, Y. Miyashita, Y. Miyoshi, I. Shinohara, M. Teramoto, J. B. Faden, A. J. Halford, M. McCarthy, R. M. Millan, J. G. Sample, D. M. Smith, L. A. Woodger, A. Masson, A. A. Narock, K. Asamura, T. F. Chang, C. Y. Chiang, Y. Kazama, K. Keika, S. Matsuda, T. Segawa, K. Seki, M. Shoji, S. W. Y. Tam, N. Umemura, B. J. Wang, S. Y. Wang, R. Redmon, J. V. Rodriguez, H. J. Singer, J. Vandegriff, S. Abe, M. Nose, A. Shinbori, Y. M. Tanaka, S. UeNo, L. Andersson, P. Dunn, C. Fowler, J. S. Halekas, T. Hara, Y. Harada, C. O. Lee, R. Lillis, D. L. Mitchell, M. R. Argall, K. Bromund, J. L. Burch, I. J. Cohen, M. Galloy, B. Giles, A. N. Jaynes, O. Le Contel, M. Oka, T. D. Phan, B. M. Walsh, J. Westlake, F. D. Wilder, S. D. Bale, R. Livi, M. Pulupa, P. Whittlesey, A. DeWolfe, B. Harter, E. Lucas, U. Auster, J. W. Bonnell, C. M. Cully, E. Donovan, R. E. Ergun, H. U. Frey, B. Jackel, A. Keiling, H. Korth, J. P. McFadden, Y. Nishimura, F. Plaschke, P. Robert, D. L. Turner, J. M. Weygand, R. M. Candey, R. C. Johnson, T. Kovalick, M. H. Liu, R. E. McGuire, A. Breneman, K. Kersten, and P. Schroeder, "The space physics environment data analysis system (SPEDAS)," Space Sci. Rev. **215**, 9 (2019).

[57] J. Burch, *Magnetospheric Multiscale Mission* (Laboratory for Atmospheric and Space Physics (LASP) at the University of Colorado, Boulder, 2015).

[58] R. C. Davidson, N. T. Gladd, C. S. Wu, and J. D. Huba, "Effects of finite plasma beta on the lower-hybrid-drift instability," Phys. Fluids **20**, 301–310 (1977).

[59] C. Norgren, A. Vaivads, Y. V. Khotyaintsev, and M. André, "Lower hybrid drift waves: Space observations," Phys. Rev. Lett. **109**, 055001 (2012).